

# Photoelectron spectroscopy of metal cluster anions: $\text{Cu}_n^-$ , $\text{Ag}_n^-$ , and $\text{Au}_n^-$

Joe Ho, Kent M. Ervin, and W. C. Lineberger

Department of Chemistry and Biochemistry, University of Colorado, and Joint Institute for Laboratory Astrophysics, University of Colorado and National Institute of Standards and Technology, Boulder, Colorado 80309-0440

(Received 22 May 1990; accepted 8 August 1990)

Negative ion photoelectron spectra of  $\text{Cu}_n^-$ ,  $\text{Ag}_n^-$  ( $n = 1-10$ ), and  $\text{Au}_n^-$  ( $n = 1-5$ ) are presented for electron binding energies up to 3.35 eV at an instrumental resolution of 6–9 meV. The metal cluster anions are prepared in a flowing afterglow ion source with a cold cathode dc discharge. In the spectra of  $\text{Cu}_2^-$ ,  $\text{Ag}_2^-$ , and  $\text{Au}_2^-$ , the  $M_2 X^1\Sigma_g^+ \leftarrow M_2^- X^2\Sigma_u^+$  transitions are vibrationally resolved. We analyze these spectra to yield the adiabatic electron affinities, vibrational frequencies, bond length changes, and dissociation energies. The  $a^3\Sigma_u^+$  triplet states of  $\text{Cu}_2$  and  $\text{Ag}_2$  are also observed. Using experimental and theoretical data, we assign the major features in the  $\text{Cu}_3^-$  and  $\text{Ag}_3^-$  spectra to the transition from the linear ground state of the anion ( $M_3^- 1\Sigma_g^+$ ) to an excited linear state of the neutral ( $M_3 2\Sigma_u^+$ ). The  $\text{Au}_3^-$  spectrum is attributed to a two-photon process, photodissociation followed by photodetachment of the  $\text{Au}^-$  or  $\text{Au}_2^-$  fragment. For larger clusters, we measure the threshold and vertical detachment energies as a function of size. Trends in the electron affinities and excited state energy levels as a function of cluster size and composition are discussed in terms of simple models.

## I. INTRODUCTION

The study of metal clusters has enjoyed explosive progress during the past decade.<sup>1-3</sup> This research spans the areas of materials science, surface chemistry, catalysis, and solid state physics. Clusters have properties intermediate between the atomic or molecular state and the solid state; cluster studies are designed to bridge gaps in our understanding of microscopic and macroscopic states.<sup>4,5</sup> Clusters may also exhibit new characteristics found in neither small molecules nor the bulk.

Metal cluster properties, structure, and reactivity have been investigated experimentally and theoretically. Properties such as ionization potentials,<sup>6-9</sup> electron affinities,<sup>10-16</sup> and electronic state energy levels<sup>10,13</sup> have been measured as a function of cluster size and compared to calculations. Detailed studies of electronic and vibrational structure have been undertaken for small clusters, primarily dimers but now including a few trimers and tetramers.<sup>1,3</sup> The spectroscopic complexity of larger metal clusters has made such studies challenging. Transition metal clusters<sup>1,17</sup> in particular have received extensive attention because of the interest in systems that have *d* electron orbitals available for bonding. Involvement of electronic configurations with partially filled *d* shells can produce a large number of low-lying electronic states, making the spectra particularly complex.

Among the transition metals, copper, silver, and gold clusters are especially attractive for study because they are relatively simple. Each of the ground state atoms has a closed *d* shell and a single *s* valence electron; hence they can be seen as "alkali-like" metals. Because of this reduced complexity, much theoretical work has been devoted to small copper-group metal clusters.<sup>17-32</sup> Gas phase spectra of neutral copper dimers and trimers have been reported.<sup>10-14,33</sup>

Negative ion laser photoelectron spectroscopy<sup>34</sup> is a powerful experimental method for the study of metal clus-

ters.<sup>15,16</sup> This technique provides the electronic and vibrational spectrum of the neutral species corresponding to the anion cluster geometry. Because the cluster anions are separated by size using a mass spectrometer, there is no ambiguity relating to the size of the cluster giving rise to the spectrum. The photoelectron spectra of coinage metal (group 11) clusters have been reported earlier by our group<sup>10</sup> ( $\text{Cu}_n^-$ ,  $n = 1-10$ ), by Smalley and co-workers<sup>15,35</sup> ( $\text{Cu}_n^-$ ,  $n = 1-410$ ;  $\text{Ag}_n^-$ ,  $n = 7-11$ ;  $\text{Au}_n^-$ ,  $n = 7-11$ ), and by Lutz and co-workers<sup>14</sup> ( $\text{Ag}_n^-$ ,  $n = 3-27$ ). The Smalley and Lutz groups employ pulsed ion sources and pulsed ultraviolet lasers for photodetachment with time-of-flight electron energy analysis, while we use a continuous ion source with a near-ultraviolet argon-ion laser for photodetachment and an electrostatic electron energy analyzer. At the present state-of-the-art, the pulsed techniques allow higher photon energies and larger clusters, while the methods used here offer better energy resolution (6–9 meV or 50–70  $\text{cm}^{-1}$ ) and are better suited for investigations of the detailed electronic and vibrational structure of smaller clusters ( $n \leq 10$ ) and for precise electron affinity determinations. In this work, we present the ultraviolet (351.1 nm or 3.531 eV) negative-ion photoelectron spectra of the coinage metal (group 11) clusters  $\text{Cu}_n^-$  and  $\text{Ag}_n^-$  ( $n = 1-10$ ) and  $\text{Au}_n^-$  ( $n = 1-5$ ). The previous report from this laboratory<sup>10</sup> involved visible (488.0 nm or 2.540 eV) photoelectron spectra of the copper clusters.

In Sec. II, we review the experimental methods used in this study, including the production of metal anion clusters. Experimental spectra are presented in Sec. III, along with the determination of electron affinities. The discussion, Sec. IV, includes an explanation of the bonding in the anion ground state and in the neutral singlet and triplet states of the dimers. A Franck–Condon analysis of the ground state dimer spectra yields vibrational constants and bond lengths.

The trimer spectra are analyzed and related to *ab initio* calculations of their geometries and electronic structure. The possible geometries for anion ground states of tetramers and pentamers are described. For larger clusters, the trends in electron affinities and electronic structure as a function of cluster size and composition are discussed.

## II. EXPERIMENTAL METHODS

The negative-ion photoelectron spectrometer and metal cluster anion source have been described in detail previously.<sup>10,36,37</sup> Metal cluster anions are produced in a flowing afterglow ion source by cathodic sputtering with a dc discharge. The ions are extracted from the flowing afterglow tube into a low pressure region. After being focused into a beam, they are mass selected by a Wien filter. The mass-selected ion beam is further focused and then enters the interaction region. There the ion beam is crossed by a high-intensity argon ion laser beam with 351.1 nm wavelength (3.531 eV), which induces photodetachment in a fraction of the anions. Photoelectrons ejected into a small solid angle are extracted perpendicularly to the ion and laser beam plane, and their kinetic energies are measured in a hemispherical electrostatic energy analyzer.<sup>36</sup> Energies of transitions between the anion and the corresponding neutral species are determined from the difference between the photon energy and the measured photoelectron kinetic energy. We shall now describe recent modifications of our apparatus and details of the experiment pertinent to the present investigations.

### A. Metal cluster anion production

The flowing afterglow metal-cluster ion source, shown in Fig. 1, is a modified version of the one described previously.<sup>10,37</sup> It employs a dc discharge at a metal cathode in a helium/argon flow. Cluster ions are produced from sputtering of the metal cathode by  $\text{Ar}^+$  and other cations, possibly followed by further clustering in the discharge plasma.

The cathode is fabricated from high purity (> 99.9%) copper, silver, or gold metal to produce the corresponding metal cluster anions. Following each use, the metal surfaces of the cathodes are regenerated by electropolishing or by

glass-bead blasting. A mixture of argon (10%–20%) in helium flows over the metal cathode at a flow tube pressure of 0.4 Torr. Ultrahigh purity (99.999%) argon gas is used directly, while 99.995% purity helium is further purified by passage through a molecular sieve trap cooled in liquid nitrogen. The carrier gas flows in around the cathode feed-through, helping to prevent the plating of metals onto the glass insulator. The cathode is negatively biased, typically at 3–5 kV with respect to the grounded flow tube, producing a discharge with a current of 10–30 mA to ground. The gas composition, flow rate, and dc voltage are adjusted to optimize the cluster anion yields. Arcing from the cathode to ground is minimized by a simple electrical ballast, consisting of a 100 k $\Omega$  resistor and a 4 H inductor connected in series with the dc power supply, as shown in Fig. 1. Approximately 20–60 W are dissipated at the metal cathode discharge; a water cooling system is therefore necessary to keep the cathode near room temperature. Cooling water flows through the metal cathode support via tubing in the electrical feed-through, and also through tubing surrounding the flow tube.

Vibrational temperatures of the anion can be estimated from hot band intensities in the photoelectron spectra. Franck–Condon analyses of the  $\text{Cu}_2^-$ ,  $\text{Ag}_2^-$ , and  $\text{Au}_2^-$  photoelectron spectra (discussed in detail in Sec. IV B 1) indicate a vibrational temperature of  $350 \pm 50$  K. We expect this vibrational temperature to be characteristic of the larger clusters as well, since all are expected to have low-frequency vibrations (50–250  $\text{cm}^{-1}$ ) which should relax easily upon collisions with the helium/argon buffer gas. Modeling the rotational contours of individual dimer vibrational transitions indicates that the most probable rotational temperature is 300–350 K. The vibrational temperature usually sets an upper limit to rotational temperature because rotational relaxation by collisions with the flow tube buffer gas is more efficient than vibrational relaxation.<sup>37,38</sup>

### B. Clusters mass spectra

Typical mass spectra of silver and gold clusters produced in the ion source are displayed in Fig. 2. The copper mass spectrum is similar to that reported by Leopold *et al.*<sup>10</sup>

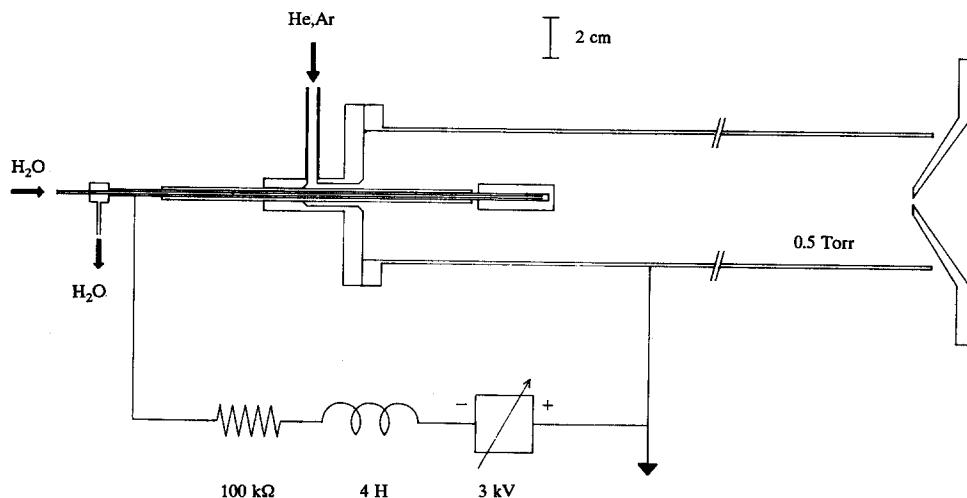


FIG. 1. Schematic diagram of the flowing afterglow system with the metal cathode discharge ion source. The scale and dimensions are approximate.

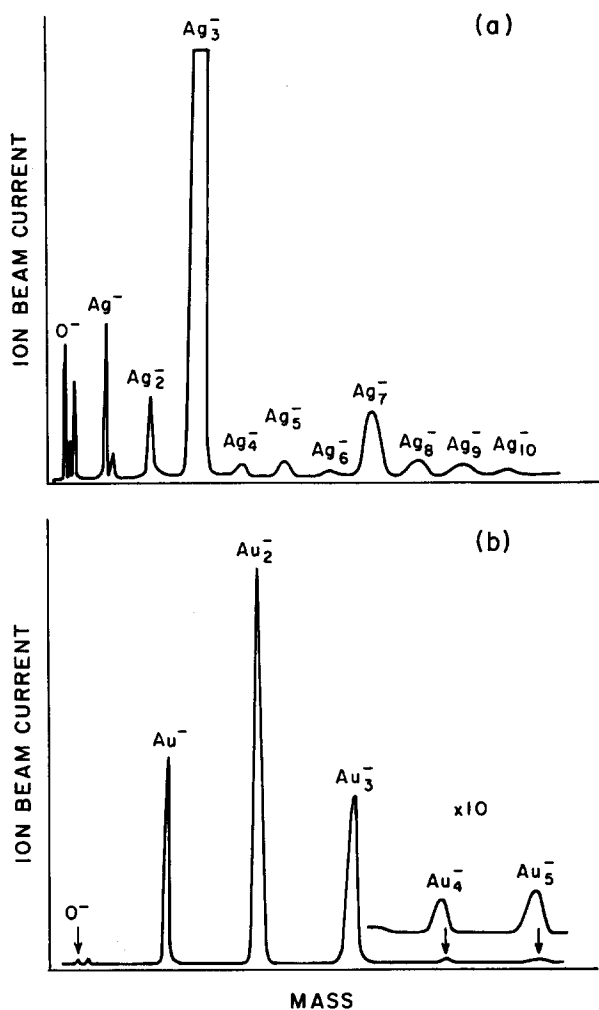


FIG. 2. Mass spectra of  $\text{Ag}_n^-$  and  $\text{Au}_n^-$  produced in the metal cathode discharge ion source. The maximum intensities are 30 pA for  $\text{Ag}_3^-$  and 60 pA for  $\text{Au}_2^-$ . The unlabeled peaks at low mass are oxide impurities.

Because of the limited mass range of our Wien filter mass selector, the mass spectra of anion clusters extend up to  $n = 10$  for copper (64 amu/atom) and silver (108 amu/atom), but only up to  $n = 5$  for gold (197 amu/atom). The most abundant cluster anion for each metal is the pentamer for copper (typically 10 pA), the trimer for silver (30 pA), and the dimer for gold (50 pA). The cluster intensity distributions of the three metals are generally reproducible, exhibiting only minor shifts of the intensity profile for different ion source conditions. Oxygen contamination is a major difficulty in producing bare metal cluster anions. Despite precautions taken to obtain pure helium and argon carrier gases and pure cathode metals, we consistently observe metal oxides such as  $\text{CuO}^-$  and  $\text{AgO}^-$  in the mass spectra. The gold cluster mass spectrum exhibits little oxide contamination. In the case of copper and silver, the smaller clusters can be resolved from the accompanying oxides. For larger clusters, the bare metal cluster anions are not sufficiently separated from their oxides because of the limited mass resolution of the Wien filter. To check for oxygen contamination, photoelectron spectra were observed at the high mass sides of sev-

eral mass peaks, as well as at the maxima of the mass peaks. In no case were oxides found to account for the features in the reported spectra, and oxide formation appears to be small for the larger clusters. Therefore, the chemical identity of the signal carrier for a mass-selected cluster is unambiguous. For more reactive transition metal anions, for example the nickel-group clusters,<sup>11</sup> oxygen contamination may cause more serious problems.

The silver mass spectrum exhibits an obvious odd > even intensity alternation, with especially large intensities for  $\text{Ag}_3^-$  and  $\text{Ag}_7^-$ . Similar phenomena have been observed in previous mass spectrometric studies<sup>8,10,12,39-41</sup> of copper group cluster anions and cations. In the present case, the intensity alternation results from the relative thermochemical stabilities of the anions, but the overall distribution is also related to the kinetic conditions in the metal sputtering source.

### C. Electron kinetic energy analysis

The electron kinetic energy scale is calibrated on the photoelectron spectra of  $\text{O}^-$ ,  $\text{S}^-$ , and  $\text{W}^-$ , as well as those of the atomic metal anions. The absolute kinetic energy is calibrated against the precisely known atomic electron affinities.<sup>42</sup> Spectra are corrected for an energy scale compression factor,<sup>36</sup> calibrated on the known energy level spacings of the tungsten atom.<sup>43</sup> The instrumental resolution function of the photoelectron spectrometer is determined by observing the shapes of atomic transitions, and can be approximated by a Gaussian with a 6–9 meV FWHM. The experimental uncertainty of the absolute electron kinetic energy of well-resolved peaks is  $\pm 0.006$  eV.

### D. Laser system

Our previous work on copper clusters<sup>10</sup> used visible laser light (458–488 nm or 2.54–2.71 eV). We have recently modified the apparatus to use near-ultraviolet light (351.1 nm or 3.531 eV), providing 1 eV higher photon energy. A detailed description of the UV laser system has been given in a recent paper,<sup>44</sup> so only a brief overview will be presented here. The UV laser system is an application of a laser stabilization scheme,<sup>45</sup> in which the output power of the argon ion laser is amplified in an optical build-up cavity<sup>46</sup> external to the laser cavity. The ion interaction region lies in the middle of the build-up cavity, which is a Fabry–Perot interferometer with high reflectivity mirrors mounted on the two sides of the vacuum chamber. Single-frequency light from the argon ion laser is injected into the build-up cavity, and at resonance the circulating power inside the cavity accumulates to a few hundred times the input laser power. The key requirement for laser power amplification is that the resonant frequencies of the laser and the build-up cavities must be exactly matched. Since both cavities have instabilities due to various sources of noise, active steps must be taken to match their resonant frequencies. A servo system locks the two cavities into resonance by adjusting the lengths of the two cavities (using piezoelectric translators on the cavity mirrors) and by fast compensation of the laser frequency using an acousto-optic modulator.

### III. RESULTS

#### A. Photoelectron spectra of copper, silver, and gold cluster anions

The 351.1 nm (3.531 eV) negative-ion photoelectron spectra of  $\text{Cu}_n^-$  and  $\text{Ag}_n^-$  ( $n = 1-10$ ) and  $\text{Au}_m^-$  ( $m = 1-5$ ) are shown in Fig. 3. The photoelectron intensities are plotted as a function of the electron binding energy, which equals the photon energy minus the measured electron kinetic energy, in the range 0.5–3.35 eV. No transitions are observed below 0.5 eV binding energy for any of the clusters, and the transmission function of the electron analyzer declines rapidly above binding energies of 3.35 eV (at low electron kinetic

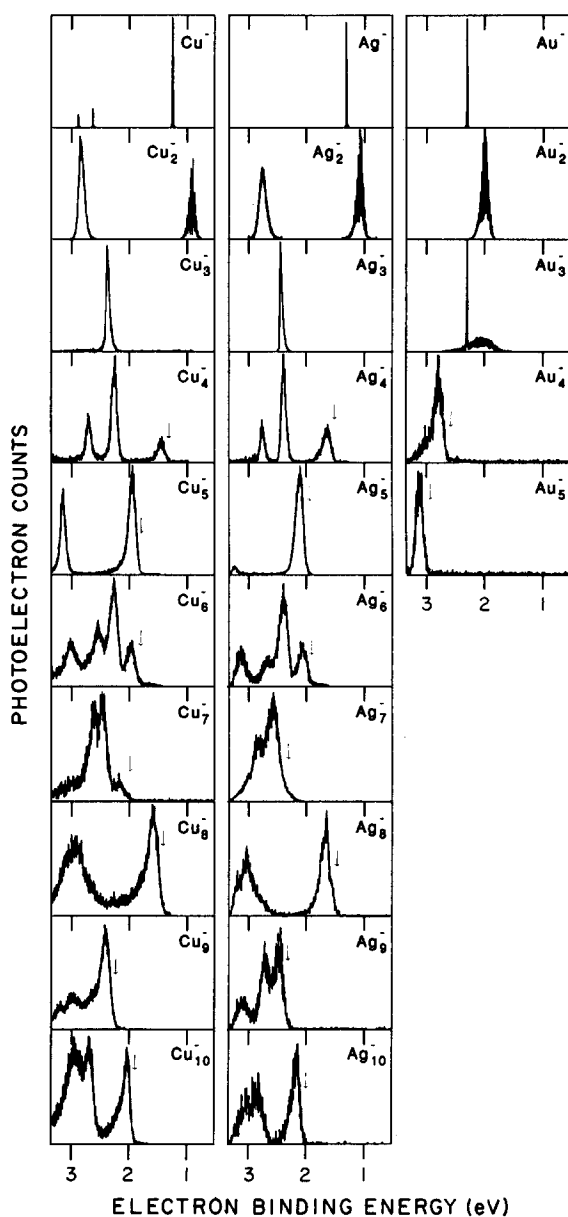


FIG. 3. Photoelectron spectra of the coinage metal anion clusters at 351.1 nm (3.53 eV) with 6–9 meV instrumental resolution. The photoelectron counts are normalized and plotted as a function of the electron binding energy, which is the photon energy minus the measured electron kinetic energy. Arrows mark the threshold binding energy  $E_T$  defined in the text.

energies). The considerable variation in signal-to-noise levels for various clusters reflects mainly different anion currents and integration times, and to a lesser extent differences in the relative photodetachment cross sections.

For the atomic species, we observe sharp transitions with widths limited by the instrumental resolution. The lowest binding energy peak in the spectrum of  $\text{Cu}^-$ , and the only peak for  $\text{Ag}^-$  and  $\text{Au}^-$ , correspond to detachment of the extra  $s$  electron in the anion,  $\text{M } ^2S(d^{10}s^1) \leftarrow \text{M}^- ^1S(d^{10}s^2)$ . For  $\text{Cu}^-$ , detachment from the  $d$  shell yields two transitions at higher binding energies within our energy range,  $\text{Cu } ^2D_{5/2}(d^9s^2) \leftarrow \text{Cu}^- ^1S(d^{10}s^2)$  and  $\text{Cu } ^2D_{3/2}(d^9s^2) \leftarrow \text{Cu}^- ^1S(d^{10}s^2)$ .

The features observed in the spectra of the dimers, trimers, and larger clusters (Fig. 3) correspond to transitions from the ground states of the anions to the ground and low-lying excited electronic states of the neutral clusters. For cluster sizes up to five atoms, each electronic band appears isolated. The spectra of larger clusters are more congested, but discrete electronic states can still be identified.

The resolution of our photoelectron spectrometer (6–9 meV or 50–70  $\text{cm}^{-1}$ ) provides the opportunity to study vibrational transitions. However, the experimental spectra (Fig. 3) show that vibrational structure is resolved only for the dimer ground-state transitions. The lack of resolved vibrational structure in the polyatomic spectra results from vibrational congestion, given the characteristic frequencies of 50–250  $\text{cm}^{-1}$  for the metal clusters and the likelihood of multiple active modes. Progressions of these modes, as well as combination bands and hot bands, contribute to the unresolved Franck–Condon profiles in the photoelectron spectra.

Dissociation and detachment are two possible outcomes of absorption of a photon by a cluster anion. Photodissociation of clusters can sometimes be detected in a sequential two-photon process in which the anionic fragment undergoes photodetachment.<sup>11</sup> Inspection of the spectra in Fig. 3 for features corresponding to smaller clusters shows no significant contributions by two photon processes, except for  $\text{Au}_3^-$  where features corresponding to  $\text{Au}^-$  and  $\text{Au}_2^-$  are observed. The gold trimer is discussed separately in Sec. IV C 3.

#### B. Electron affinities and transition energies

The adiabatic electron affinity (EA) is defined as the energy of the origin transition between the ground state of the anion and the ground state of the neutral. Photoelectron spectra yield precise values for adiabatic electron affinities when the origin can be identified. For the atomic species, the electron affinity corresponds to the  $\text{M } ^2S(d^{10}s^1) \leftarrow \text{M}^- ^1S(d^{10}s^2)$  transition. Electron affinities for Cu, Ag, and Au determined from the energies of these transitions (calibrated against  $\text{O}^-$  and  $\text{W}^-$ ) are in good agreement with previous measurements:<sup>10,47</sup>  $\text{EA}(\text{Cu}) = 1.235 \pm 0.005$  eV,  $\text{EA}(\text{Ag}) = 1.302 \pm 0.007$  eV, and  $\text{EA}(\text{Au}) = 2.30863 \pm 0.00003$  eV. (Therefore, the atomic photoelectron spectra could be used for calibration of the cluster spectra.) Since vibrational transitions are resolved for the ground electronic

states of the dimers, we can determine their electron affinities precisely from the *assigned* vibrational origin ( $\nu' = 0 \leftarrow \nu'' = 0$ ) peaks. The assignment of the vibrational origins and corrections for sequence bands and rotational broadening are discussed in detail in Sec. IV B 1. The resulting electron affinities are given in Table I.

For the clusters larger than dimer, no vibrational structure is resolved (Fig. 3). If the geometries of anion and neutral states were known, the position of the vibrational origin within the overall Franck–Condon profile of each transition could be estimated with accuracy not much less than that for vibrationally resolved spectra. Unfortunately, there is little experimental or theoretical geometry information available on clusters with  $n \geq 4$ . Therefore, we do not attempt to determine the adiabatic electron affinity (EA), but rather take an empirical approach and cite vertical detachment energies (VDE, defined as the electron binding energy at the peak of the lowest electronic transition) and the threshold binding energies ( $E_T$ , the low binding energy onset of photodetachment). These values are listed in Table I. The VDEs are relatively unambiguous in the present work because most of the electronic transitions involve discrete, resolved bands. One expects VDE to approach EA for large clusters, where the geometries of the anion and neutrals are expected to be similar. The determination of the threshold binding energy is admittedly arbitrary because it depends on the shape of the Franck–Condon profile of the transition. For consistency, we choose  $E_T$  as the energy where the intensity reaches 10% of the peak intensity. With this definition,  $E_T$  is relatively insensitive to the contributions of hot bands and to the signal-to-noise levels of individual spectra. The error bars in Table I are based solely on uncertainties in determining the defined onset due to the noise level of the baseline.

The actual positions of the vibrational origins within the observed Franck–Condon profiles depend on the geometry change and the extent of hot bands. If the anion and neutral

geometries are similar, the adiabatic electron affinity will generally fall between  $E_T$  and VDE. If the geometry or isomeric structure of the ground-state anion is very different from that of the ground-state neutral, on the other hand, it is possible that no detachment at all would be observed in the vicinity of the adiabatic transition, in which case  $E_T$  would be higher than the adiabatic electron affinity. If an electron hot band were present, it could be mistaken for the ground-state transition, which would cause  $E_T$  to be lower than the adiabatic electron affinity. However, one would expect electronic hot bands to be weak under the present experimental conditions and to change intensity with changes in the ion source conditions. No such indications of electronic hot bands are observed in the spectra reported here.

Our experimental values for VDE and  $E_T$  are generally consistent with other reports<sup>13–15,35,48</sup> within the error limits. This agreement is encouraging given the arbitrary nature of assigning  $E_T$ , and indicates that the same structural isomers are being produced in the various experiments despite the very different ion source conditions. An exception to the general agreement arises for  $\text{Ag}_5^-$ , for which the value of  $E_T$  reported by Lutz and co-workers,<sup>14,48</sup>  $E_T = 1.30 \pm 0.30$  eV, is considerably lower than ours,  $E_T = 1.93 \pm 0.06$  eV. The difference arises from an additional weak feature that was observed<sup>14,48</sup> at binding energies lower than our lowest transition. We carefully checked this energy region in the photoelectron spectra of  $\text{Cu}_5^-$ ,  $\text{Ag}_5^-$ , and  $\text{Au}_5^-$ , and observed no transitions. We suspect that an electronic hot band or an impurity accounts for the weak transition observed by Lutz and co-workers.<sup>14</sup>

Vertical detachment energies for higher electronic transitions are listed in Table II. These vertical energies are determined from the intensity maxima of the transitions. Bandwidths for isolated transitions are given in Table II as well. In the dimers, the band profile widths are 110–130 meV

TABLE I. Cluster ground state transition energies.

n	$\text{Cu}_n$			$\text{Ag}_n$			$\text{Au}_n$		
	$E_T$ (eV) <sup>a</sup>	VDE (eV) <sup>b</sup>	FWHM (meV) <sup>c</sup>	$E_T$ (eV) <sup>a</sup>	VDE (eV) <sup>b</sup>	FWHM (meV) <sup>c</sup>	$E_T$ (eV) <sup>a</sup>	VDE (eV) <sup>b</sup>	FWHM (meV) <sup>c</sup>
2		$0.88 \pm 0.02$	110		$1.06 \pm 0.02$	120		$2.01 \pm 0.01$	130
3	$2.27 \pm 0.10$	$2.37 \pm 0.01$	60	$2.36 \pm 0.01$	$2.43 \pm 0.01$	40	3.4–3.95	> 3.5	
4	$1.32 \pm 0.10$	$1.45 \pm 0.05$	145	$1.51 \pm 0.10$	$1.65 \pm 0.05$	155	$2.60 \pm 0.10$	$2.79 \pm 0.05$	155
5	$1.82 \pm 0.05$	$1.94 \pm 0.05$	140	$1.98 \pm 0.05$	$2.11 \pm 0.05$	150	$2.93 \pm 0.10$	$3.12 \pm 0.05$	140
6	$1.81 \pm 0.10$	$1.96 \pm 0.05$	160	$1.92 \pm 0.10$	$2.06 \pm 0.05$	165			
7	$1.98 \pm 0.15$	$2.16 \pm 0.10$	165	$2.30 \pm 0.10$	$2.55 \pm 0.10^d$	180 <sup>d</sup>			
8	$1.41 \pm 0.10$	$1.57 \pm 0.05$	165	$1.48 \pm 0.10$	$1.65 \pm 0.05$	160			
9	$2.25 \pm 0.10$	$2.40 \pm 0.05$	165	$2.32 \pm 0.10$	$2.48 \pm 0.10$	165			
10	$1.91 \pm 0.10$	$2.03 \pm 0.05$	145	$2.03 \pm 0.10$	$2.16 \pm 0.05$	155			
$\infty^e$		4.65			4.26			5.10	

<sup>a</sup> Threshold detachment energy ( $E_T$ ), defined as the electron binding energy where the intensity reaches 10% that of the lowest maximum.

<sup>b</sup> Vertical detachment energy (VDE), the electron binding energy of the maximum of the lowest electronic transition.

<sup>c</sup> Width (FWHM) of the lowest electronic transition.

<sup>d</sup> If the tail on the right shoulder of the  $\text{Ag}_7$  transition is a separate transition as seen for  $\text{Cu}_7$ , then  $\text{VDE} \approx 2.3$ – $2.4$  eV and  $\text{FWHM} < 180$  meV.

<sup>e</sup> Bulk work function of polycrystalline metals, Ref. 62.

TABLE II. Cluster excited state transition energies.

<i>n</i>	Excited state <sup>a</sup>	Cu <sub><i>n</i></sub>			Ag <sub><i>n</i></sub>		
		VDE(eV) <sup>b</sup>	<i>T<sub>v</sub></i> (eV) <sup>c</sup>	FWHM (meV) <sup>d</sup>	VDE(eV) <sup>b</sup>	<i>T<sub>v</sub></i> (eV) <sup>c</sup>	FWHM (meV) <sup>d</sup>
2	1	2.81	1.93	120	2.76	1.70	120
4	1	2.25	0.80	110	2.39	0.74	100
	2	2.69	1.24	110	2.76	1.11	110
5	1	3.14	1.20	120	3.22	1.10	130
6	1	2.30	0.34	150	2.39	0.33	160
	2	2.53	0.57	165	2.65	0.59	180
	3	3.00	1.04	180	3.12	1.06	170
7	1	2.45	0.29	155	2.82	0.27	> 180
	2	2.62	0.46	160			
8	1	2.93	1.36	> 180	3.02	1.17	> 180
9	1	2.60	0.20	> 180	2.71	0.23	165
	2	2.99	0.59	> 180	3.11	0.63	> 180
10	1	2.69	0.66	155	2.82	0.65	170
	2	2.93	0.90	> 180	3.06	0.89	> 180

<sup>a</sup> Excited state transition, where the ground state is labeled 0.

<sup>b</sup> Vertical detachment energy (VDE) is the electron binding energy at the peak maximum.

<sup>c</sup> Vertical term energy,  $T_v = \text{VDE}(\text{excited state}) - \text{VDE}(\text{ground state})$ .

<sup>d</sup> Transition width.

(FWHM) for both the ground-state and the first excited-state transitions. For clusters  $n \geq 4$ , the widths of the lowest energy transitions are almost constant, with values of 135–165 meV. The trimers of copper and silver are exceptional, exhibiting much narrower widths. The measured positions of the first excited states of Cu<sub>*n*</sub> and Ag<sub>*n*</sub> are in good agreement with other reports.<sup>13,48</sup>

## IV. DISCUSSION

### A. Overview

The coinage-metal cluster spectra share several common characteristics. The cluster spectra exhibit a small number of discrete and separated low-lying electronic states. Although larger clusters have increasing numbers of observed transitions, the density of states is still not large. The spectra for corresponding copper and silver clusters are remarkably similar, both in structure and absolute transition energies. The values of VDE and  $E_T$  for Cu<sub>*n*</sub> and Ag<sub>*n*</sub> are almost the same, especially for larger clusters, but the values for gold clusters are consistently about 1 eV higher than their Cu<sub>*n*</sub> and Ag<sub>*n*</sub> counterparts. Although the energy range limits the number of low-lying states that can be observed for gold clusters, the lowest transitions are similar to copper and silver except for the energy shift.

These observations may be qualitatively explained by the simple valence electron configuration of the constituent atoms of the clusters. Each atom in the clusters contributes a single *s* valence electron, while the *d* shell is fully occupied. Interactions among the *s* electrons dominate the bonding and electronic structure in the clusters.<sup>30,49</sup> The limited number of ways these atomic orbitals (AOs) can be combined to form bonding molecular orbitals (MOs) gives rise to the small number of low-lying electronic states. The interactions of the *s* AOs are quite similar for copper and silver, which have  $3d^{10}4s^1$  and  $4d^{10}5s^1$  atomic configurations, re-

spectively. The *s* electron bonding characteristics in gold,  $4f^{14}5d^{10}6s^1$  are also similar, but valence orbital contractions due to the filled *f* shell and relativistic effects cause a shift of the electron binding energies to higher values.<sup>50</sup> Specific features of the clusters of various sizes are discussed individually in the following sections.

### B. Dimers

The photoelectron spectra of copper, silver, and gold dimers are illustrated in Fig. 3. The peaks at lower electron binding energy for Cu<sub>2</sub> and Ag<sub>2</sub>, and the only peak for Au<sub>2</sub>, correspond to the ground state transition,  $M_2 X^1\Sigma_g^+ \leftarrow M_2^- X^2\Sigma_u^+$ . These bands display clear vibrational structure, as indicated in the expanded portions of the spectra reproduced in Fig. 4. Bands at higher electron binding energy in the Cu<sub>2</sub> and Ag<sub>2</sub> spectra show only broad profiles without resolved vibrational structure. These transitions are assigned to the triplet excited states of the neutral dimer,  $a^3\Sigma_u^+$ . For Au<sub>2</sub>, the  $a^3\Sigma_u^+$  state transition is beyond our energy range.

#### 1. Singlet ground state

A complete discussion of the vibrational spectrum of ground-state Cu<sub>2</sub> was given in an earlier paper.<sup>10</sup> The present experiment has the advantage of better instrumental resolution and a lower vibrational temperature, allowing improved molecular constants to be obtained. We now present a detailed discussion of the vibrational analysis of the Cu<sub>2</sub>  $X^1\Sigma_g^+ \leftarrow Cu_2^- X^2\Sigma_u^+$  transition as an example, followed by brief descriptions of the silver and gold dimer results.

In the ground-state electronic band of Cu<sub>2</sub>, Fig. 4, a vibrational progression with the 265 cm<sup>-1</sup> frequency<sup>1</sup> spacing of the neutral dimer is observed starting at the peak at a binding energy of 0.84 eV. Hot bands are observed at lower energies with the 200 cm<sup>-1</sup> anion vibrational frequency spacing.

The change in frequency spacing at the peak at 0.84 eV initially identifies it as the  $\nu' = 0 \leftarrow \nu'' = 0$  origin transition.

A Franck–Condon spectral simulation is employed to extract molecular parameters from the photoelectron spectrum. Franck–Condon factors are calculated for Morse oscillators using numerical integration vibrational wavefunctions obtained analytically by the Laguerre-series recursion method.<sup>51</sup> This procedure gives more accurate Franck–Condon factors for high vibrational states than does the previously used<sup>10</sup> Hutchisson method, in which anharmonic corrections to harmonic oscillator Franck–Condon factors are calculated by a perturbation treatment. The effective linewidths are 11–12 meV FWHM, which includes the instrumental resolution of 6–9 meV, broadening due to vibrational sequence and hot bands, and rotational broadening. The rotational contour is generated using rotational constants for the initial- and final-state geometries and the usual selection rules and Hönl–London factors for a  $\Sigma$ – $\Sigma$  electronic transition.<sup>52</sup> The calculated rotational line spectrum is then convoluted with the instrumental resolution function. The resulting contours are convoluted with the vibrational line strengths from the Franck–Condon calculation and used to fit the experimental spectrum by an iterative nonlinear least-squares optimization. This procedure explicitly accounts for shifts in the position of the origin peak due to rotational broadening and vibrational sequence bands.

In our simulation, the molecular parameters of the neutral  $\text{Cu}_2 X^1\Sigma_g^+$  are fixed at known experimental values.<sup>1</sup> The adjustable parameters in the Franck–Condon fit are the anion vibrational constants ( $\omega_e''$  and  $\omega_e x_e''$ ), the anion bond length ( $r_e''$ ), the energy position of the origin, and the vibrational and rotational temperatures of the anion. The optimized fit to the data is shown in Fig. 4. Shifting the origin to the left or right by one vibrational quantum results in poor fits (i.e., the sum of squared residuals increases by a factor of 3–4), confirming the origin assignment. The position of the origin gives an electron affinity of  $\text{EA}(\text{Cu}_2) = 0.836 \pm 0.006$  eV. Other molecular constants obtained for the anion are shown in Table III. These results agree with our previous work<sup>10</sup> within experimental uncertainties. The optimized anion vibrational temperature is  $T_{\text{vib}} = 350 \pm 25$  K and the rotational temperature is  $T_{\text{rot}} \approx 330$  K.

The photoelectron spectrum of  $\text{Ag}_2$  is strikingly similar to that of  $\text{Cu}_2$  (Figs. 3 and 4). A Franck–Condon analysis as described for  $\text{Cu}_2^-$  yields the electron affinity,  $\text{EA}(\text{Ag}_2) = 1.023 \pm 0.007$  eV, and molecular constants for  $\text{Ag}_2^-$  given in Table III. In this case, the neutral bond length is not known with certainty; therefore, the Franck–Condon analysis can only estimate the change in the bond length upon photodetachment.

The  $\text{Au}_2$  photoelectron spectrum and the Franck–Condon simulation are shown in Fig. 4. Because the anion and neutral dimers have similar vibrational frequencies, simple inspection of the spectrum does not provide an unambiguous origin assignment for the gold dimer. However, the Franck–Condon simulations show that only the assigned origin (Fig. 4) gives a good fit to the data. The electron affinity obtained

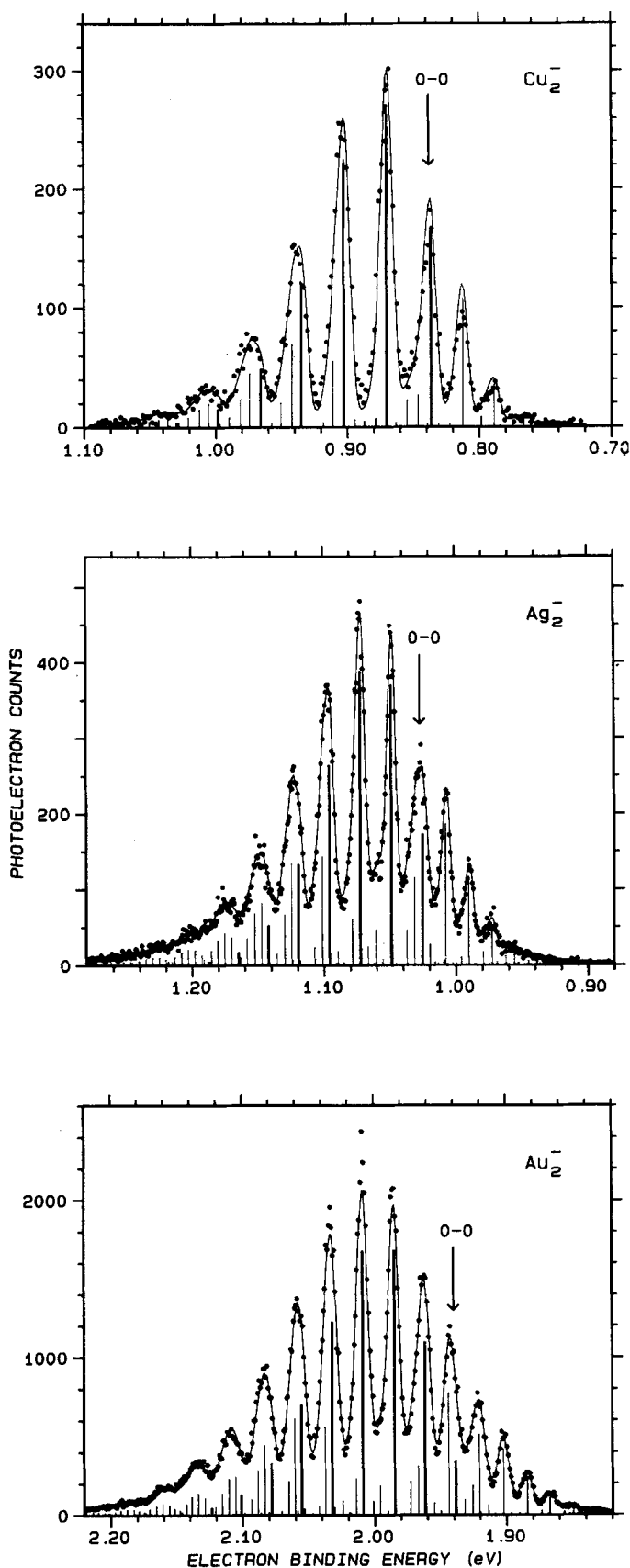


FIG. 4. Ground-state transitions in the photoelectron spectra of  $\text{Cu}_2^-$ ,  $\text{Ag}_2^-$ , and  $\text{Au}_2^-$ . The points represent the experimental data and solid lines are Franck–Condon simulations. Transitions from the ground vibrational state of the anion are given by thick sticks and transitions from vibrationally hot anions by thin sticks. Arrows mark the vibrational origin transitions.

TABLE III. Molecular constants of copper, silver, and gold dimers.<sup>a</sup>

Species	$\omega_e$ (cm <sup>-1</sup> )	$\omega_e x_e$ (cm <sup>-1</sup> )	$r_e$ (Å)	$D_0$ (eV)	$T_0$ (eV)	EA (eV)
Cu <sub>2</sub> <sup>-</sup> X <sup>2</sup> Σ <sub>u</sub> <sup>+</sup>	196 ± 15	[0.7]	2.343 ± 0.007	1.62 ± 0.20	0.0	
Cu <sub>2</sub> X <sup>1</sup> Σ <sub>g</sub> <sup>+</sup>	266.43	1.035	2.2197	2.02 ± 0.08	0.0	0.836 ± 0.007
Cu <sub>2</sub> a <sup>3</sup> Σ <sub>u</sub> <sup>+</sup>	[120 ± 25]		[2.55]	[0.10]	[1.92]	
Ag <sub>2</sub> <sup>-</sup> X <sup>2</sup> Σ <sub>u</sub> <sup>+</sup>	145 ± 10	[0.9]	$r'_e + 0.124 \pm 0.007^b$	1.37 ± 0.16	0.0	
Ag <sub>2</sub> X <sup>1</sup> Σ <sub>g</sub> <sup>+</sup>	192.4	0.60	$r'_e^b$	1.65 ± 0.03	0.0	1.023 ± 0.007
Ag <sub>2</sub> a <sup>3</sup> Σ <sub>u</sub> <sup>+</sup>				[0]	[<1.74]	
Au <sub>2</sub> <sup>-</sup> X <sup>2</sup> Σ <sub>u</sub> <sup>+</sup>	149 ± 10	[0.7]	2.582 ± 0.007	1.92 ± 0.15	0.0	
Au <sub>2</sub> X <sup>1</sup> Σ <sub>g</sub> <sup>+</sup>	190.9	0.42	2.4719	2.29 ± 0.02	0.0	1.938 ± 0.007

<sup>a</sup> Values from this work except *neutral ground-state* vibrational constants, bond lengths, and dissociation energies from Morse (Ref. 1). Values in brackets are estimates (see the text).

<sup>b</sup> An uncertain assignment gives  $r'_e = 2.480$  Å [V. I. Srdanov and D. S. Pestic, *J. Mol. Spectrosc.* **90**, 27 (1981)].

from the simulation is EA(Au<sub>2</sub>) = 1.938 ± 0.007 eV. Other derived molecular parameters are given in Table III.

## 2. Potential energy curves

Before discussing the triplet excited state spectra of Cu<sub>2</sub> and Ag<sub>2</sub>, it is useful to discuss the potential energy curves for the dimer neutrals and anions. Figure 5 presents approximate potential energy curves for Cu<sub>2</sub> and Cu<sub>2</sub><sup>-</sup>, constructed from literature values for the neutral bond energy and bond length, and electron affinities and anion molecular constants obtained in this work. Potential energy curves for silver and

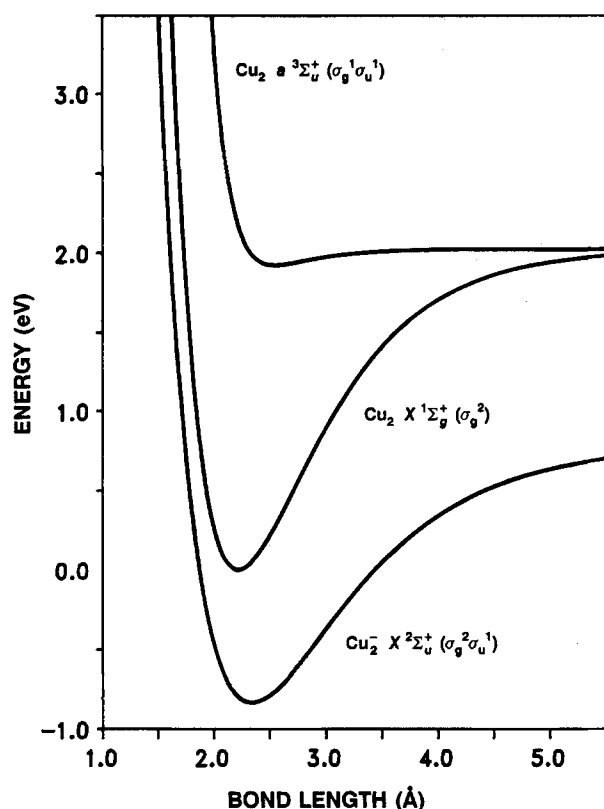


FIG. 5. Qualitative potential energy curves for Cu<sub>2</sub><sup>-</sup> X<sup>2</sup>Σ<sub>u</sub><sup>+</sup>, Cu<sub>2</sub> X<sup>1</sup>Σ<sub>g</sub><sup>+</sup>, and Cu<sub>2</sub> a<sup>3</sup>Σ<sub>u</sub><sup>+</sup>.

gold dimers are similar. The bonding in the coinage metal dimers involves primarily the valence *s* electrons.<sup>22,26</sup> The two *s* AOs form a bonding σ<sub>g</sub> MO and an antibonding σ<sub>u</sub><sup>\*</sup> MO. The resulting electronic states and configurations are M<sub>2</sub><sup>-</sup> X<sup>1</sup>Σ<sub>u</sub><sup>+</sup>(*ns*σ<sub>g</sub>)<sup>2</sup>(*ns*σ<sub>u</sub><sup>\*</sup>)<sup>1</sup>, M<sub>2</sub> X<sup>1</sup>Σ<sub>g</sub><sup>+</sup>(*ns*σ<sub>g</sub>)<sup>2</sup>, and M<sub>2</sub><sup>\*</sup> a<sup>3</sup>Σ<sub>u</sub><sup>+</sup>(*ns*σ<sub>g</sub>)<sup>1</sup>(*ns*σ<sub>u</sub><sup>\*</sup>)<sup>1</sup>. The formal bond order is one-half for the anion ground state, one for neutral singlet ground state, and zero for the neutral triplet state. Thus, one might expect that the anion would have a much smaller dissociation energy than the ground singlet state, and that the excited triplet would not be bound. However, the bond orders given by this simple MO model do not adequately reflect the bond strengths for the diatomic molecules of transition metals.<sup>53</sup> Actually, the anion bond energies exceed 80% of the neutral singlet bond energies (Table III).

These observations show that the simple *ns* orbital bonding picture is not entirely adequate, as has been pointed out previously for other transition metal dimer ions.<sup>10,53,54</sup> The contributions of the (*n* - 1)*d* and *np* orbitals to the *ns*σ MOs must also be considered.<sup>20,21</sup> For copper, silver, and gold, the (*n* - 1)*d* shell is fully occupied and thus has little direct influence on the bonding, but *np* orbitals are available and have energies near the *ns* orbitals. According to *ab initio* calculations by Bauschlicher *et al.*<sup>22</sup> for Cu<sub>2</sub>, the 4*s*σ<sub>u</sub><sup>\*</sup> orbital is extensively polarized by mixing in 4*p* orbital character. This polarization decreases the electron density between the two nuclei, reducing the anti-bonding character of the 4*s*σ<sub>u</sub><sup>\*</sup> orbital. Hence, the bond energy of the anion is nearly as strong as the (4*s*σ<sub>g</sub>)<sup>2</sup> neutral singlet. According to this explanation, we can also expect that the (4*s*σ<sub>g</sub>)<sup>1</sup>(4*s*σ<sub>u</sub><sup>\*</sup>)<sup>1</sup> neutral triplet might be weakly bound rather than repulsive, despite the formal bond order of zero. These arguments apply as well to Ag<sub>2</sub> and Au<sub>2</sub>, since the *s* and *p* orbitals have similar energies in each case and can therefore mix effectively in forming molecular orbitals.

## 3. Triplet excited state

The a<sup>3</sup>Σ<sub>u</sub><sup>+</sup> triplet states of the neutral dimers are less well characterized than the ground singlet states. Bondybey<sup>55</sup> has reported observation of the Cu<sub>2</sub> a<sup>3</sup>Σ<sub>u</sub><sup>+</sup>

$\rightarrow \text{Cu}_2 X^1\Sigma_g^+$  transition by laser-induced fluorescence of  $\text{Cu}_2$  isolated in a solid neon matrix and found that the  $a^3\Sigma_u^+$  state is bound by  $1000\text{--}1500\text{ cm}^{-1}$ . His analysis of the Franck–Condon profile of the observed emission band gave estimates of  $r'_e = 2.48 \pm 0.03\text{ \AA}$  and  $\omega'_e \approx 125 \pm 25\text{ cm}^{-1}$  for the  $a$  state.

The excited-state transition peaks in our spectra exhibit broad profiles with no vibrational structure. The intensity maximum of this broad peak lies at  $2.81 \pm 0.05\text{ eV}$  binding energy for  $\text{Cu}_2 a^3\Sigma_u^+$  ( $1.97\text{ eV}$  above the origin of  $\text{Cu}_2^1\Sigma_g^+$ ) and at  $2.76 \pm 0.05$  for  $\text{Ag}_2$  ( $1.74\text{ eV}$  above the ground-state origin). The triplet-state transition for the gold dimer is not observed; assuming the gold dimer triplet is also about  $2\text{ eV}$  above the ground state, it is well beyond our energy range.

The lack of vibrational structure in the triplet-state transitions can be explained by two factors. First, the triplet state is weakly bound, so the potential well is very shallow and the vibrational frequencies are probably small compared to our instrumental resolution ( $50\text{--}70\text{ cm}^{-1}$ ). The presence of hot bands would further increase vibrational congestion. Second, since the equilibrium bond length of the  $a^3\Sigma_u^+$  state is longer than that of the anion  $X^2\Sigma_u^+$  state, the vertical transition to the  $a^3\Sigma_u^+$  surface may be in the continuum region. Since the singlet and triplet states share the same dissociation asymptote (see Fig. 5), the ground state dissociation energy is an upper limit for the triplet-state term energy (assuming the triplet is at least weakly bound). For  $\text{Cu}_2$ , the triplet vertical detachment energy is  $1.97 \pm 0.05\text{ eV}$  above the singlet origin, while the neutral bond energy<sup>1</sup> is  $2.02 \pm 0.08\text{ eV}$ . Therefore, the detachment we observe likely corresponds to bound–bound transitions at lower electron binding energies, but to bound–free transitions on the high-energy side of the peak. In the case of  $\text{Ag}_2$ , the vertical detachment energy of the triplet state is  $1.74 \pm 0.05\text{ eV}$  above the vibrational origin of the neutral ground state, but the dissociation energy of the neutral ground state<sup>1</sup> is only  $1.65 \pm 0.03\text{ eV}$ . This indicates that the observed band corresponds largely to bound-to-continuum transitions.

The shape of the transition envelope contains information about the potential energy curve of the upper state.<sup>56</sup> However, the profiles are significantly complicated by the presence of vibrational hot bands, and we have made no attempt to deconvolute the bound–free spectra. If the  $\text{Cu}_2 a^3\Sigma_u^+$  state is assumed to be at least weakly bound, then the Franck–Condon simulation program can be employed to calculate bound–bound transitions. In this simulation, the parameters of the anion ground state are fixed from the Franck–Condon fit to the ground-state transition. The simulation yields  $r'_e \approx 2.55\text{ \AA}$  and  $\omega'_e \approx 120\text{ cm}^{-1}$  for  $\text{Cu}_2 a^3\Sigma_u^+$ , with a transition origin in the vicinity of  $2.76\text{ eV}$  binding energy. The bond length and frequency are in reasonable agreement with Bondybey's estimates.<sup>55</sup> However, this fitting method gives only a rough estimate because individual transitions are not resolved and because the Franck–Condon factor calculation does not treat transitions to the continuum region above the  $\text{Cu}_2$  dissociation asymptote. Therefore, the precise assignment of the origin is uncertain. The simulation indicates that the triplet state vibrational frequency can be

no larger than  $150\text{ cm}^{-1}$ , since otherwise vibrational structure would be resolved under our conditions.

### C. Trimers

#### 1. Electronic states and geometries of neutrals and anions

Copper, silver, and gold trimers have been recently studied by *ab initio* methods.<sup>22–24</sup> The energy levels of anion and neutral states of copper trimer are illustrated in Fig. 6. Three low-lying electronic states are found for the neutral trimers:  $^2B_2$  (acute isosceles triangle),  $^2A_1$  (obtuse isosceles triangle), and  $^2\Sigma_u^+$  (linear). The  $^2B_2$  and  $^2A_1$  states arise from a Jahn–Teller distortion of a doubly degenerate  $^2E'$  state of equilateral triangle geometry.<sup>23,24</sup> In the  $^2E'$  state, the electronic configuration is  $(a'_1)^2(e')^1$ , where  $a'_1$  is a bonding combination of three s AOs and  $e'$  is a doubly degenerate nonbonding orbital.<sup>22</sup> The  $^2B_2$  state is always lower in energy than the  $^2A_1$ , since the apex atoms can mix in some  $p$  orbital character and thereby increase bonding.<sup>24</sup> However the  $^2B_2$  and  $^2A_1$  states are nearly degenerate, with calculated energy differences of only  $59\text{ cm}^{-1}$  for  $\text{Cu}_3$ ,  $108\text{ cm}^{-1}$  for  $\text{Ag}_3$ , and  $130\text{ cm}^{-1}$  for  $\text{Au}_3$ .<sup>25,26</sup> The linear  $^2\Sigma_u^+$  ( $(\sigma_g)^2(\sigma_u)^1$ ) state is less stable than the  $^2E'$  state by  $0.23$ ,  $0.05$ , and  $0.09\text{ eV}$  for  $\text{Cu}_3$ ,  $\text{Ag}_3$ , and  $\text{Au}_3$ , respectively, according to *ab initio* calculations.<sup>24</sup>

The electronic states of the anionic trimers are comparatively less well characterized. Early calculations found that the  $\text{Ag}_3^-$  has a linear ground state.<sup>27</sup> Later Leopold *et al.*<sup>10</sup> suggested that  $\text{Cu}_3^-$  might also have linear geometry. Recent calculations indicate that the ground states of all three coin-

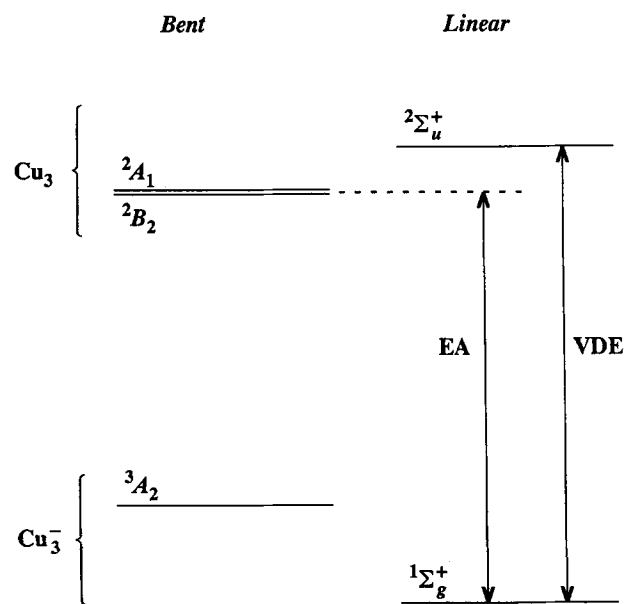


FIG. 6. Schematic potential energy levels for the anion and neutral trimers. The adiabatic electron affinity (EA) corresponds to the transition between the linear ground state of the anion and the bent ground state of the neutral. The vertical detachment energy (VDE) corresponds to the linear-to-linear transition ending in an excited state of the neutral.

age metal trimer anions are linear.<sup>23,24</sup> The linear  ${}^1\Sigma_g^+$  ground state anion has a  $(\sigma_g)^2(\sigma_u)^2$  configuration. The bonding  $\sigma_g$  MO is a symmetric combination of the three valence  $s$  AOs. The  $\sigma_u$  MO is an antisymmetric combination of the two terminal  $s$  AOs mixed with  $p$  orbital character on the central atom, making it partially bonding. The linear  ${}^2\Sigma_u^+(\sigma_g)^2(\sigma_u)^1$  neutral state is formed by detaching an electron from the  $\sigma_u$  orbital of the linear anion state. The lowest bent state of the anion trimer is  ${}^3A_2'(a_1)^2(e')^2$ , which has  $D_{3h}$  symmetry. This state is formed by attaching an extra electron to the  $e'$  orbital of the bent neutral molecule. Since the  $\sigma_u$  orbital in linear geometry is basically bonding, while the  $e'$  orbital in bent geometry is nonbonding, the linear geometry ( ${}^1\Sigma_g^+$ ) is favored for the anion ground state.<sup>24</sup> Theoretical calculations<sup>22,24,25</sup> find that the linear geometry is more stable than the bent structure, by 0.51 eV for  $\text{Cu}_3^-$ , 0.85 eV for  $\text{Ag}_3^-$  and 1.1 eV for  $\text{Au}_3^-$ .

## 2. $\text{Cu}_3$ and $\text{Ag}_3$

The photoelectron spectra of  $\text{Cu}_3$  and  $\text{Ag}_3$  (Fig. 3) are very similar, each exhibiting a single transition. Expanded portions of these transitions are displayed in Fig. 7. The line widths of copper and silver trimer transitions are about 60 and 40 meV, respectively, less than half the average values for dimers and other higher clusters. The peaks are asymmetric, showing a tail on the side of low electron binding

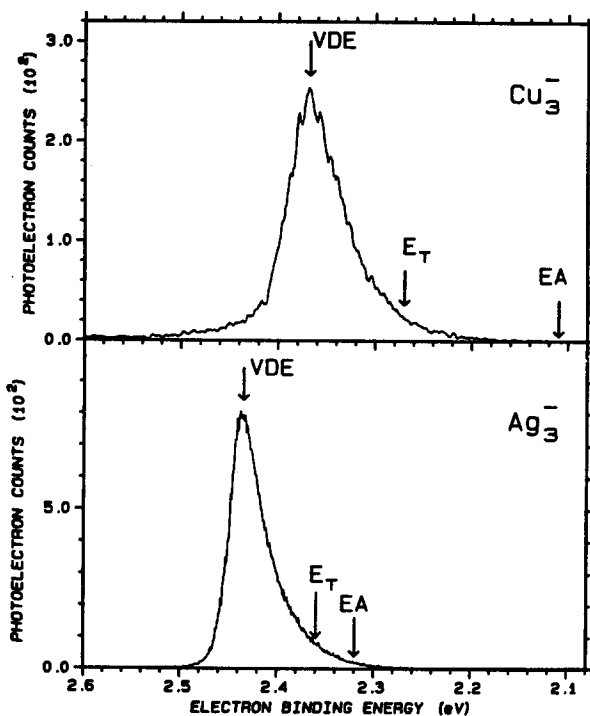


FIG. 7. Expanded portions of photoelectron spectra of  $\text{Cu}_3^-$  and  $\text{Ag}_3^-$ . The vertical detachment energies (VDE) and threshold binding energy ( $E_T$ ) are defined in the text. Estimated adiabatic electron affinities (EA) are estimated from the experimental vertical detachment energy (corresponding to the transition from linear ground state of the anion to the linear excited state of the neutral) and the theoretical energy splittings between the bent ground state of the neutral and its excited linear state (see the text).

energy, but no vibrational structure is resolved. The vertical detachment energies, corresponding to the intensity maxima of the peaks, are  $\text{VDE}(\text{Cu}_3) = 2.37 \pm 0.01$  eV and  $\text{VDE}(\text{Ag}_3) = 2.43 \pm 0.01$  eV.

Given the electronic states of the neutral and anion molecules described above, there are several possible transitions in our spectrum. According to the Franck–Condon principle, the strongest band should be either a linear-to-linear or a bent-to-bent transition. Also, the width of the electron detachment peak reflects the magnitude of geometry change during the transition. From the observed narrowness of the transitions, relative to the dimer and larger cluster spectra, the geometry change between the anion and the neutral must be small. More quantitatively, the Franck–Condon profile widths can be estimated for various electronic transitions using *ab initio* geometries.<sup>24</sup> The bond length change is predicted to be small for the transition between linear symmetric states ( $M_3 \tilde{a}^2\Sigma_u^+ \leftarrow M_3^- \tilde{X}^1\Sigma_g^+$ ), from 2.377 to 2.348 Å for copper and from 2.754 to 2.732 Å for silver. The longer bond length in each case is that of the anion. The predicted change<sup>26</sup> for the bent-to-bent transition ( ${}^2E' \leftarrow \tilde{a}^3A_2'$ ) for copper is from 2.462 to 2.417 Å (equilateral triangle geometry). Using these calculated geometries, we carried out Franck–Condon simulations for these two transitions. The results indicate that the observed narrow peak widths are consistent with the geometry changes from *ab initio* calculations only for the linear-to-linear transition.<sup>57</sup> The simulated profile of the bent-to-bent transition would be further broadened by consideration of the Jahn–Teller distortion and energy splitting in  $\text{Cu}_3$ . Therefore, we conclude that the observed major feature is due to the linear-to-linear transition. This conclusion is also consistent with the theoretical prediction that  $\text{Cu}_3^-$  and  $\text{Ag}_3^-$  have linear ground-state geometries. Therefore, we assign the main features of the spectra to  $M_3 \tilde{a}^2\Sigma_u^+ \leftarrow M_3^- \tilde{X}^1\Sigma_g^+$  transitions. Because the ground state of the neutral is *not* linear, the observed bands do not correspond to the adiabatic electron affinity.

The Franck–Condon simulation indicates that the peak maximum (VDE) in the vertical linear-to-linear transition corresponds closely to the vibrational origin,  $\nu' = 0 \leftarrow \nu'' = 0$ . Thus, the adiabatic electron affinity, defined as the energy for the transition between the anion and neutral ground states,  $M_3 \tilde{X}^2B_2 \leftarrow M_3^- \tilde{X}^1\Sigma_u^+$ , can be estimated from

$$\text{EA}(M_3) = \text{VDE}(M_3) - T_0(M_3^2\Sigma_u^+),$$

where  $T_0$  is the energy of the linear  ${}^2\Sigma_u^+$  state above the  ${}^2B_2$  ground state of the neutral. The term energies are not known experimentally, but have been calculated<sup>25,26</sup> to be 0.26 eV for  $\text{Cu}_3$  and 0.11 eV for  $\text{Ag}_3$ . Using these theoretical values and taking the vertical detachment energy from experiment (Table I), we obtain the following estimates for the adiabatic electron affinities:  $\text{EA}(\text{Cu}_3) \approx 2.11$  eV and  $\text{EA}(\text{Ag}_3) \approx 2.32$  eV. The uncertainty of these EAs depends primarily on the (unknown) accuracy of the theoretical term energies.

The Franck–Condon simulations for the linear-to-linear transitions fail to fit the asymmetric low energy side of the observed bands. These tails on the  $\text{Cu}_3^-$  and  $\text{Ag}_3^-$  peaks

can be explained by  $M_3 \tilde{X}^2B_2 \leftarrow M_3 \tilde{X}^1\Sigma_g^+$  transitions from the populated vibrational levels of the linear atom terminating in excited bending vibrational states of the neutral bent trimer. The Franck–Condon intensity of the vibrational origin is small because of the extreme change in the geometry ( $180^\circ$  to  $60^\circ$ ). Qualitative Franck–Condon simulations show that the  $\nu' = 0$  to  $\nu'' = 0$  transition is many orders of magnitude too weak to be observed under the present experimental conditions. However, transitions to highly excited bending vibrational levels of the bent neutral trimer should have significant Franck–Condon factors. The exact shape of the Franck–Condon profile for this transition depends on the details of the potential energy surface connecting the bent and linear geometries. A recent study<sup>23</sup> of the potential energy surface of  $Ag_3$  and  $Au_3$  indicated that the  $^2B_2$  and  $^2A_1$  surfaces have energy barriers which separate the linear and bent geometries. The  $^2B_2$  saddle point is nearly flat for  $Ag_3$  and correlates with the ground linear state, while the  $^2A_1$  surface has a high barrier and correlates to an excited linear state. Assuming that the  $Cu_3$  surfaces are similar to those of  $Ag_3$ , we expect transitions to excited levels of the  $^2B_2$  surface in both cases to occur at binding energies below the vertical detachment energy for the linear neutral state, consistent with the observed tails.

In our previous photoelectron spectrum of  $Cu_3^-$  in the visible,<sup>10</sup> a weak peak was observed at lower electron binding energies,  $VDE \approx 1.5$  eV. This peak was assigned to an electronic hot band, originating from the bent excited state of the anion,  $^3A'_2$ . A corresponding feature is not observed in the present work, presumably due to cooler ion source conditions. Transitions from this anion state to the  $^2B_2$  or  $^2A_1$  neutral state have favorable Franck–Condon factors. The width of the low-energy peak,<sup>10</sup> 140 meV, is much broader than the main transition. The width is consistent with the predicted geometry change<sup>22</sup> for the  $Cu_3 \tilde{X}^2B_2 \leftarrow Cu_3^- \tilde{a}^3A'_2$  bent-to-bent transition. The theoretical estimate<sup>22</sup> of the vertical transition energy is  $1.54 \pm 0.10$  eV, in excellent agreement with the observed value of 1.5 eV.

### 3. $Au_3$

The  $Au_3^-$  photoelectron spectrum is quite different from that of  $Cu_3^-$  or  $Ag_3^-$ . Comparing the spectra in Fig. 3 and the VDE values in Table I for copper, silver, and gold clusters, one would expect the ground-state transition of  $Au_3^-$  to have a vertical detachment energy about 1.1 eV higher than those of  $Cu_3^-$  and  $Ag_3^-$ , giving  $VDE(Au_3) \approx 3.5$  eV. This would place the transition beyond our experimental energy range. Bauschlicher<sup>24</sup> has predicted  $EA(Au_3) = 3.93$  eV based on calculated energies scaled to experimental results for Au and  $Au_2$ . A recent preliminary report by Smalley and co-workers<sup>15</sup> gives  $EA(Au_3) \approx 3.9$  eV.

The  $Au_3$  spectrum in Fig. 8 consists of two features that appear to superimpose the spectra of the monomer and dimer. The photoelectron intensity is much weaker than for  $Au^-$ ,  $Au_2^-$ ,  $Cu_3^-$ , or  $Ag_3^-$ . Laser power measurements show a quadratic intensity dependence of the electron signal

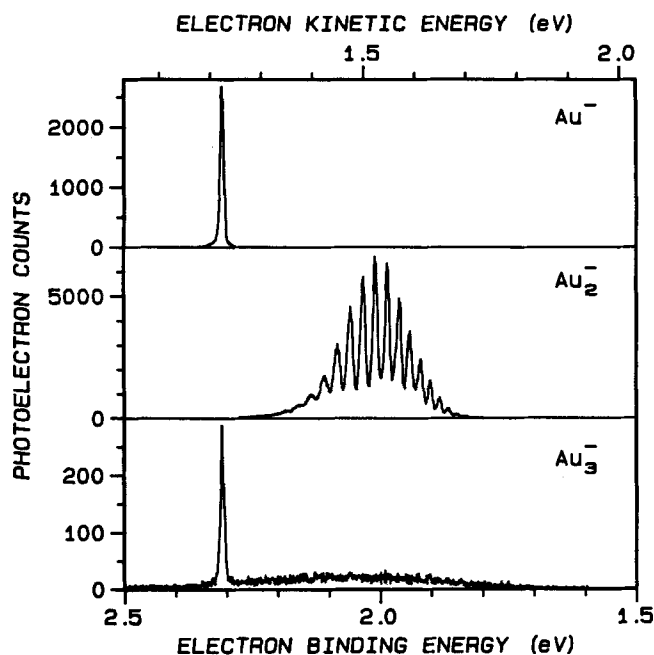
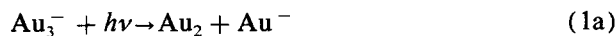


FIG. 8. Photoelectron spectra of  $Au^-$ ,  $Au_2^-$ ,  $Au_3^-$ . The trimer spectrum comprises two features with small photodetachment cross sections. The sharp feature corresponds to atomic gold, via a two-photon process in which photodissociation,  $Au_3^- + h\nu \rightarrow Au^- + Au_2$  is followed by photodetachment,  $Au^- + h\nu \rightarrow Au + e^-$ . The broad feature is assigned to  $Au_2^-$  in an analogous two-photon process in which  $Au_2^-$  is produced by the initial photodissociation.

for both trimer features, although this measurement was not definitive in the case of the dimer-like feature because of low signal levels. Based on these observations, we assign the features in the  $Au_3^-$  spectrum to two-photon processes occurring within the 50 ns time the ions require to pass through the laser beam. The sharp feature clearly corresponds to  $Au^-$  photodetachment, via a sequential two-photon process in which photodissociation of the trimer anion to  $Au^-$  is followed by its photodetachment,



and



This feature lies exactly at the position expected for photodetachment of free  $Au^-$ . The small, broad feature is assigned to  $Au_2^-$  in the analogous two photon process,



and



The breadth of the transition and lack of resolved vibrations indicate that the  $Au_2^-$  intermediate is extremely hot vibrationally, consistent with the expectation for  $Au_2^-$  formed by photodissociation of  $Au_3^-$ . An alternative assignment of the broad feature in the  $Au_3$  spectrum to an electronically excited state of the anion trimer (rather than to  $Au_2^-$  in a two-photon process) can be ruled out based on comparison to the

energy spacing of the excited trimer in  $\text{Cu}_3^-$ , and on theoretical detachment energy,<sup>24</sup> both of which indicate the observed vertical detachment energy is much too low for the linear excited state of  $\text{Au}_3^-$ .

Relative total cross sections for the various processes are obtained by normalizing the integrated photoelectron counts for each transition by the ion current, laser power, and integration time, expressed relative to the detachment probability for  $\text{Au}^-$ . The values for the two features in the trimer spectrum ( $P_1 = 0.004$  and  $P_2 = 0.017$ , respectively) are much smaller than for either the monomer ( $P_{1b} \equiv 1.0$ ) or dimer ( $P_{2b} = 1.4$ ), as obtained from the corresponding single photon spectra. The ratio of  $P_1$  to  $P_2$  indicates that the cross section for the initial photodissociation to produce  $\text{Au}_2^- + \text{Au}$ , Eq. (2a), is three to four times larger than the cross section for dissociation to produce  $\text{Au}_2 + \text{Au}^-$ , Eq. (1a).

Because the photon energy is smaller than the electron affinity of  $\text{Au}_3$ , only the photodissociation channel is energetically accessible with one photon. For all other clusters examined, photodetachment is energetically allowed. In the  $\text{Cu}_3^-$  and  $\text{Ag}_3^-$  spectra, no photofragmentation is observed although both dissociation and detachment are energetically accessible at  $h\nu = 3.531$  eV. There is always a competition between dissociation and electron detachment upon photoabsorption of negative-ion clusters. When energetically allowed, photodetachment is usually the dominant process and photofragmentation is a minor process, as has been noted previously.<sup>10,12</sup>

#### D. Tetramers and higher clusters

The assignment of geometries for the ground states of transition metal cluster anions and neutrals larger than trimers is difficult because the number of low-lying electronic states increases rapidly with increasing cluster size. We shall draw upon comparisons with the alkali metal clusters,<sup>15,16,48,65</sup> which have received extensive experimental attention and are more tractable for theoretical studies. For small anionic clusters, a linear geometry is energetically favorable because it tends to minimize the charge repulsion for the extra electron at the end of the chain.<sup>58</sup> For large clusters, on the other hand, we can expect little change in the geometry upon addition of an electron to the neutral cluster. The tetramer and pentamer may fall between these two classes.

The alkali-like tetramer anions have been assumed to have either rhombic or linear structures in the ground state. A recent study of  $\text{Na}_4^-$  concludes that a linear arrangement is somewhat more likely than the rhombus.<sup>58</sup> Hückel calculations<sup>59</sup> suggest that both  $\text{Cu}_4$  and  $\text{Cu}_4^-$  have rhombic geometry. An *ab initio* calculation of  $\text{Au}_4$  indicates that the anion ground state is  $^1A_1$  with rhombic geometry.<sup>28</sup> Our spectra of  $\text{Cu}_4$  and  $\text{Ag}_4$  show three transition peaks. The widths of the two excited-state peaks are 110–120 meV and the symmetric peak shapes indicate that they probably arise from single electronic transitions. If we assume a linear geometry for the anion ground state, then the three peaks can be assigned to  $^1\Sigma_g^-$ ,  $^3\Sigma_g^-$ , and  $^3\Sigma_u^+$  states of the neutral. Experiments<sup>48</sup> at 6.4 eV photon energy reveal at least three ad-

ditional peaks within 3 eV of the origin in the  $\text{Ag}_4^-$  spectrum. The calculation<sup>28</sup> of  $\text{Au}_4$  low-lying electronic states finds only two linear states,  $^1\Sigma_g^+$  and  $^3\Sigma_g^-$  in a 5 eV energy range, but it finds three rhombic and two square states within a 3 eV range above the rhombic ground state. The rhombic and square geometries are close, so transitions between them would have significant Franck–Condon overlap. Another recent calculation also favors the rhombic structure for ground state  $\text{Cu}_4$ .<sup>60</sup> It is reasonable to assume that  $\text{Cu}_4^-$ ,  $\text{Ag}_4^-$ , and  $\text{Au}_4^-$  have the same ground states and similar energy spacings of their low-lying excited states. Therefore we favor assigning rhombic geometry to all of the tetramer anions. The three observed peaks can then be tentatively assigned to neutral ground state  $^1A_1$ , and excited states  $^3B_1$  and  $^1B_2$ . These assignments are far from certain, however, because of the number of low-lying structures.

According to a recent calculation,<sup>58</sup> the most stable structure of  $\text{Na}_5^-$  is the trapezoidal planar form similar to the predicted neutral structure; pentamer anions are also predicted to have low-lying pyramidal and  $D_{5h}$  structures.<sup>59</sup> Recent theoretical work, which compared the calculated and experimental electron affinities and electron energy levels, suggest that the parallel trapezoid structure is most likely for the  $\text{Cu}_5^-$  ground state.<sup>60</sup> We tentatively assign the trapezoidal planar geometry to the ground state of both the anion and neutral of the coinage metal pentamers. The two peaks would then be assigned to  $^2A_1$  and  $^2B_1$ , respectively. But one cannot exclude with certainty the possibility of linear or other structures for the anion ground state.

Our assignments above for tetramers and pentamers are far from certain, and need further confirmation from both experiment and theory. Insufficient information exists about the geometries of larger clusters to attempt assignment of the transitions. The agreement of the present photoelectron spectra with those obtained from laser vaporization sources<sup>14,15,35</sup> indicates that the same structural isomer is being produced under entirely different source conditions, which further implies that there is an energetically isolated, most stable structure for copper-group cluster anions.

#### E. Thermochemistry

Since the EAs of the atoms and dimers are precisely determined by photoelectron spectroscopy, the relation

$$D_0(\text{M}_2^-) = D_0(\text{M}_2) + \text{EA}(\text{M}_2) - \text{EA}(\text{M}) \quad (3)$$

can be employed to determine the anion dissociation energy. The dissociation energies of the neutral dimers are taken from Morse's review.<sup>1</sup> The derived values of  $D_0(\text{M}_2^-)$  are listed in Table III.

The dissociation energies of the trimer anion can be determined by

$$D_0(\text{M}_2 - \text{M}^-) = \text{EA}(\text{M}_3) + D_0(\text{M}_2 - \text{M}) - \text{EA}(\text{M}) \quad (4)$$

and

$$D_0(\text{M}_2^- - \text{M}) = \text{EA}(\text{M}_3) + D_0(\text{M}_2 - \text{M}) - \text{EA}(\text{M}_2), \quad (5)$$

using atomic and dimer EAs for copper and silver from our experiment (Table I), and dissociation energies of the neutral trimers derived from experimental atomization energies for trimers<sup>61</sup> and dissociation energies of the neutral dimers.<sup>1</sup> The results are listed in Table IV. The dissociation energies of the anion trimers are twice as large as those of the corresponding neutral trimers. This behavior is in accord with the molecular orbital picture, namely that the extra electron occupies a bonding orbital in linear geometry. The stability of this orbital is also reflected by the  $M_3$  electron affinity, which is the highest of all clusters up to ten atoms.

The observation of the dissociation process (2a) implies that  $D_0(\text{Au}_2^- - \text{Au}) < 3.5$  eV. From Eq. (5), this sets an upper limit on the electron affinity,  $\text{EA}(\text{Au}_3) < 3.95$  eV. Since direct photodetachment is not observed, the vertical detachment energy of the most probable linear-to-linear transition is greater than the photon energy of 3.531 eV. Because the  $\text{Au}_3$   $^2\Sigma_u^+$  state is calculated<sup>24</sup> to be 0.16 eV above the  $\text{Au}_3$   $^2B_2$  ground state, this yields  $\text{EA}(\text{Au}_3) > 3.4$  eV. We therefore estimate  $\text{EA}(\text{Au}_3)$  is in the range 3.4–3.95 eV. A recent preliminary experimental report<sup>15</sup> gives  $\text{EA}(\text{Au}_3) \approx 3.9$  eV. *Ab initio* work<sup>24</sup> predicts the  $\text{EA}(\text{Au}_3) = 3.93$  eV and  $\text{VDE}(\text{Au}_3) = 4.14$  eV. These values are in good agreement with the limits obtained here.

## F. Cluster properties vs cluster size

### 1. Electron affinities

Electron affinities as a function of cluster size are shown in Fig. 9. The electron affinities of metal cluster anions must approach the metal bulk work function as their size increases. The work functions<sup>62</sup> of polycrystalline copper, silver, and gold are 4.65, 4.26, and 5.10 eV, respectively. Although we observe an overall increase in electron affinity with increasing cluster size, the electron affinities of the cluster anions examined here are far from the bulk values. A recent experiment<sup>35</sup> which examined extremely large copper clusters shows that the electron affinity is about 4 eV for  $n = 410$ , indicating that the approach to the work function is extremely gradual.

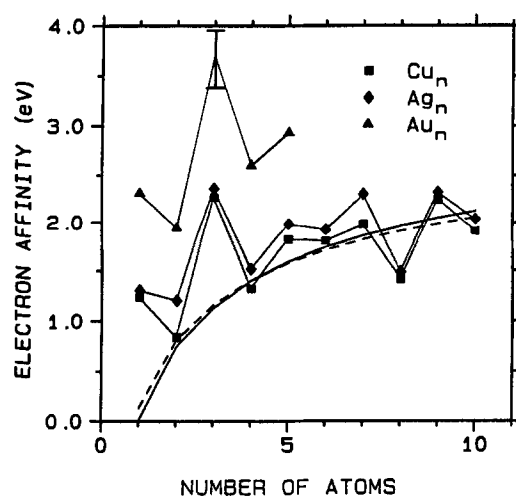


FIG. 9. The experimental electron affinities are shown as a function of the cluster size. The lines represent the prediction of the spherical drop model for  $\text{Cu}_n$  (solid) and  $\text{Ag}_n$  (dashed) with the parameters given in the text.

The electrostatic “spherical drop” model,<sup>63</sup> in which the metal clusters are treated as perfect conducting spheres, has been used to explain the size dependence of cluster electron affinities. The interaction between the detached electron and the image charge in the sphere leads to the following prediction about the electron affinity of the cluster

$$\text{EA} = \text{WF} - (5/8)e^2/R, \quad (6)$$

where WF is the work function of the bulk metal,  $e$  is the electronic charge, and  $R$  is the effective sphere radius. The radius can be estimated by  $R = n^{1/3}r_0 + \delta r$ , where  $r_0$  is half the average distance between atoms in the solid and  $\delta r$  compensates for the “extension” of the electron density beyond the cluster radius.<sup>10</sup> Theoretical considerations<sup>64</sup> indicate that  $r_0$  should be 80%–100% of the bulk internuclear separation and  $\delta r$  should be in the range of  $1-2a_0$ , where  $a_0$  is the Bohr radius. For  $\text{Cu}_n^-$  and  $\text{Ag}_n^-$ , the spherical drop model is in reasonable agreement with the experimental data for  $r_0 = 1.41$  Å for  $\text{Cu}_n$  and  $r_0 = 1.65$  Å for  $\text{Ag}_n$  and

TABLE IV. Electron affinities and dissociation energies of Cu, Ag, and Au trimers (eV).

Quantity	Transition	$\text{Cu}_3$	$\text{Ag}_3$	$\text{Au}_3$	Ref.
Vertical detachment energy	$^2\Sigma_u^+ \leftarrow ^1\Sigma_g^+$	$2.37 \pm 0.01$	$2.43 \pm 0.01$	$> 3.5$ 3.9	This work 15
Adiabatic electron affinity	$^2B_2 \leftarrow ^1\Sigma_g^+$ <sup>expt.</sup> theory	2.11 <sup>a</sup> 2.21	2.32 <sup>a</sup> 2.33	$> 3.4, < 3.95$ 3.93	This work 22,24
$D_0(M_2 - M)$		$1.08 \pm 0.19$	$0.97 \pm 0.16$	$1.51 \pm 0.15$	1
$D_0(M_2 - M^-)^b$		1.96	1.99	3.1 <sup>d</sup>	This work
$D_0(M_2^- - M)^c$		2.35	2.27	3.5 <sup>d</sup>	This work

<sup>a</sup> Derived from the experimental VDE and the theoretical  $M_3$   $^2\Sigma_u^+ < M_3$   $^2B_2$  energy difference (Ref. 22).

<sup>b</sup> Derived from Eq. (7).

<sup>c</sup> Derived by Eq. (8).

<sup>d</sup> Derived using theoretical value of  $\text{EA}(\text{Au}_3) = 3.93$  eV (Ref. 24).

$\delta r = a_0$ .<sup>10,48</sup> Curves with these values in Eq. (6) are drawn in Fig. 9 for comparison. Using the same parameters for copper, the EA( $\text{Cu}_{4,10}$ ) is calculated to be 3.85 eV, compared to the experimental value of 4 eV.<sup>35</sup> Thus Eq. (6) appears to describe rather well the gross trends in the electron affinities of large clusters as a function of size.

Another major feature in the dependence of electron affinities on cluster size is the strong alternation between even and odd numbered clusters. This alternation has been observed for the alkali<sup>65</sup> and coinage metal clusters.<sup>10,13,14</sup> The ionization potentials have the opposite alternation pattern (even > odd) for alkali and coinage metal clusters.<sup>8,66</sup> The alternation in EAs is essentially an electron pairing effect, resulting from the circumstance that each atom in the cluster contributes a single valence electron to the bonding orbitals.<sup>18,67</sup> Even anion clusters have an odd total ( $n + 1$ ) of valence electrons and the HOMO (highest occupied molecular orbital) is singly occupied; odd anion clusters have an even number of electrons with two electrons in the HOMO. The electron in a doubly occupied HOMO will feel a stronger effective core potential because the electron screening is less effective for electrons in the same orbital than for inner shell electrons. Thus the binding energy of a valence electron within an odd anion cluster is larger than that of an even one. The opposite alternation pattern for ionization potentials provides supporting evidence for this argument, since the cations have an odd number of valence electrons for even clusters. The alkali metal clusters show similar alternation patterns in their electron affinities. Bowen and co-workers<sup>16,65</sup> have made detailed comparisons of the electron affinities and electronic states as a function of cluster size for clusters of K [Ar] $s^1$  and Cu [Ar] $d^{10}s^1$  atoms.

## 2. HOMO-LUMO gap

The energy levels of the lowest excited neutral states can provide information about the energy gaps between the HOMO and the LUMO (lowest unoccupied molecular orbital) for the clusters.<sup>10,13</sup> When there is an even number of atoms, the HOMO of the ground state is always doubly occupied and the first excited state should be associated with the HOMO-LUMO transition if the orbitals are nondegenerate. For example, the two peaks in the  $\text{Cu}_2$  spectrum correspond to transitions terminating on the ground state  $X^1\Sigma_g^+(4s\sigma_g)^2$  and first excited state  $a^3\Sigma_u^+(4s\sigma_g)(4s\sigma_u^*)$ . For the ground state,  $(4s\sigma_g)$  is the HOMO and  $4s\sigma_u^*$  is the LUMO. Thus, the energy difference between the two peaks corresponds to the HOMO-LUMO energy gap. This assignment can be extended to the other even clusters. For odd clusters the HOMO is singly occupied in the neutral, so that the energy level of the first excited state corresponds to the difference between the two highest occupied orbitals.

Figure 10 shows the first excited-state energies of even clusters as a function of cluster size. The energy gap between the lowest neutral states, which we equate with the HOMO-LUMO band gaps, decreases rapidly with increasing cluster size in the first three even clusters, but the gap jumps sharply at the octamer and resumes the decline for the decamer. Energy gaps in copper and silver clusters of the same size are

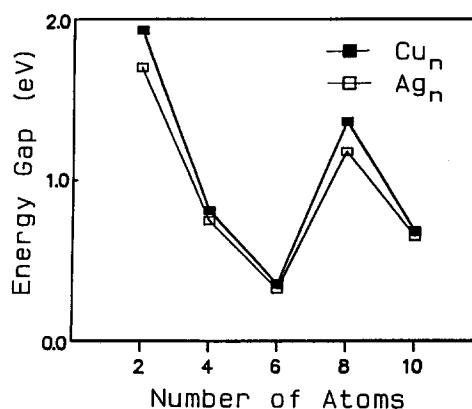


FIG. 10. HOMO-LUMO energy gaps for even-numbered copper and silver clusters.

almost the same, reflecting their similar electronic properties. Pettiette *et al.*<sup>13</sup> have measured the HOMO-LUMO energy gap of copper clusters in the 6–40 atom range. Our data are in agreement with theirs for 6–10 atoms. As the clusters become very large, the HOMO-LUMO gap is expected to vanish as the lower excited states evolve into the conduction band. A recent study<sup>35</sup> of much larger copper clusters ( $n = 1-410$ ) shows the approach to bulk copper band structure.

## 3. Jellium shell model

The jellium or shell model has been successfully applied to describe metal cluster electronic properties, particularly for alkali and coinage metal clusters.<sup>13,41,68,69</sup> The model was first applied to the intensity discontinuities in the mass spectra of alkali clusters<sup>68,69</sup> and coinage metal clusters.<sup>40,41</sup> Recently the model has been extended to calculate the ionization potentials, electron affinities, and energy levels of excited states of metal clusters.<sup>13,48,70</sup> The shell model also describes the even/odd alternation in electron affinities and ionization potentials.

According to the shell model, the first main shell closing is expected at  $n = 8$ . The eight valence electrons of an octamer fully fill the  $S^2P^6$  electron shell, so the extra electron of the anion octamer starts a new shell and is relatively weakly bound. This prediction of the shell model is consistent with the relatively low electron affinity of the octamer, and the special stability of the closed shell can also explain the large HOMO-LUMO gap for the octamer. Nevertheless, it is questionable whether the jellium model is physically reasonable for clusters in the small size class examined here, because the assumption of uniform charge in a spheroidal cluster must break down for sufficiently small metal clusters.

## V. CONCLUSION

Negative-ion photoelectron spectra of the coinage metal clusters  $\text{Cu}_n^-$ ,  $\text{Ag}_n^-$  ( $n = 1-10$ ), and  $\text{Au}_n^-$  ( $n = 1-5$ ) have been observed with 351.1 nm (3.531 eV) laser light at an instrumental resolution of 6–9 meV. These experiments provide direct information on low-lying electronic states of the mass-selected neutral metal clusters.

The electronic structure of corresponding copper, silver, and gold clusters is remarkably similar. The electron affinities of  $\text{Cu}_n$  and  $\text{Ag}_n$  are nearly the same, while those of  $\text{Au}_n$  are consistently about 1 eV higher. The EAs generally increase with increasing cluster size; this behavior can be explained by the electrostatic drop model, which accounts for the size dependence of the EA relative to the bulk work function. The EA values also alternate strongly between even- and odd-numbered clusters, with the EAs for even-numbered clusters being smaller than for neighboring clusters. This phenomenon is related to electron pairing effects, which may be described either by a shell-type model or by a molecular orbital model. Photodetachment of even-numbered anions occurs by removal of an unpaired electron, which is relatively easier than for neighboring odd clusters, for which a doubly occupied orbital must be broken.

The photodetachment transitions for the diatomic species are vibrationally resolved. Franck-Condon simulations for these spectra yield molecular constants of the neutrals and anion diatoms, as well as adiabatic electron affinities. The weakly bound neutral triplet state  $a^3\Sigma_u^+$ , is also observed in  $\text{Cu}_2$  and  $\text{Ag}_2$ . The experimental results support the theoretical calculation<sup>22</sup> that the antibonding character of the  $(\sigma_u^*)$  orbital is reduced by mixing with  $p$  orbitals.

The  $\text{Cu}_3$  and  $\text{Ag}_3$  spectra exhibit a single peak; the peak width is relatively narrower than for the other clusters, which indicates a small change in geometry between the anion and neutral. This feature is assigned to a linear-to-linear transition from the  $\tilde{X}^1\Sigma_g^+$  linear ground state of the anion to the  $^2\Sigma_u^+$  linear excited state of the neutral. The vertical detachment energies are in agreement with *ab initio* calculations.<sup>24</sup> The  $\text{Au}_3$  spectrum is determined to be a combination of atomic and diatomic spectra, a result of two-photon processes in which photodissociation is followed by photodetachment of the  $\text{Au}^-$  and  $\text{Au}_2^-$  fragments.

Higher clusters exhibit discrete, isolated electronic bands. The simplicity of the spectra reflects the limited number of low-lying electronic states that can be formed from the single  $s$  valence electron on each atom. In contrast, nickel group clusters,<sup>11</sup> for which each atom has a hole in the  $d$  shell, have a large density of low-lying electronic states yielding highly congested photoelectron spectra. Tentative geometry and electronic state assignments for the tetramers and pentamers can be made by comparison to alkali metal clusters and to theoretical calculations.

## ACKNOWLEDGMENTS

We thank Mary K. Gilles for expert experimental assistance. Richard Weppner fabricated the metal cathodes. This research was supported by the National Science Foundation, Grants CHE88-19444 and PHY86-04504.

<sup>1</sup> M. D. Morse, *Chem. Rev.* **86**, 1049 (1986).

<sup>2</sup> M. Moskovits, *Metal Clusters* (Wiley, New York, 1986).

<sup>3</sup> M. M. Kappes, *Chem. Rev.* **88**, 369 (1988).

<sup>4</sup> A. W. Castleman, Jr. and R. G. Keese, *Acc. Chem. Res.* **19**, 413 (1986).

<sup>5</sup> R. E. Smalley, in *Comparison of Ab Initio Quantum Chemistry with Ex-*

*periment: State of the Art*, edited by R. J. Bartlett (Reidel, New York, 1985).

<sup>6</sup> R. L. Whetten, M. R. Zakin, D. M. Cox, D. J. Trevor, and A. Kaldor, *J. Chem. Phys.* **85**, 1697 (1986).

<sup>7</sup> E. A. Rohlfing, D. M. Cox, A. Kaldor, and K. H. Johnson, *J. Chem. Phys.* **81**, 3846 (1984); E. A. Rohlfing, D. M. Cox, and A. Kaldor, *ibid.* **81**, 4497 (1984).

<sup>8</sup> D. E. Powers, S. G. Hansen, M. E. Geusic, D. L. Michalopoulos, and R. E. Smalley, *J. Chem. Phys.* **78**, 2866 (1983).

<sup>9</sup> K. LaiHing, P. Y. Cheng, and M. A. Duncan, *Z. Phys. D* **13**, 161 (1989).

<sup>10</sup> D. G. Leopold, J. Ho, and W. C. Lineberger, *J. Chem. Phys.* **86**, 1715 (1987).

<sup>11</sup> K. Ervin, J. Ho, and W. C. Lineberger, *J. Chem. Phys.* **89**, 4514 (1988); J. Ho, K. M. Ervin, and W. C. Lineberger (to be published).

<sup>12</sup> L. S. Zheng, C. M. Karner, P. J. Brucat, S. H. Yang, C. L. Pettiette, M. J. Craycraft, and R. E. Smalley, *J. Chem. Phys.* **85**, 1681 (1986).

<sup>13</sup> C. L. Pettiette, S. H. Yang, M. J. Craycraft, J. Conceicao, R. T. Laaksonen, O. Cheshnovsky, and R. E. Smalley, *J. Chem. Phys.* **88**, 5377 (1988).

<sup>14</sup> G. Ganteför, M. Gausa, K.-H. Meiwes-Broer, and H. O. Lutz, *Faraday Discuss. Chem. Soc.* **88**, 16 (1988).

<sup>15</sup> O. Cheshnovsky, C. L. Pettiette, and R. E. Smalley, in *Ion and Cluster Ion Spectroscopy and Structure*, edited by J. P. Maier (Elsevier, Amsterdam, 1988), p. 330.

<sup>16</sup> S. T. Arnold, J. G. Eaton, D. Patel-Misra, H. W. Sarkas, and K. H. Bowen, in *Ion and Cluster Ion Spectroscopy and Structure*, edited by J. P. Maier (Elsevier, Amsterdam, 1988), p. 417.

<sup>17</sup> J. Koutecký and P. Fantucci, *Chem. Rev.* **86**, 539 (1986); W. Weltner, Jr. and R. J. VanZee, *Annu. Rev. Phys. Chem.* **35**, 291 (1984).

<sup>18</sup> J. L. Gole and W. C. Stwalley, *Metal Bonding and Interactions in High Temperature Systems: with Emphasis on Alkali Metals*, ACS Symp. Ser. **179** (American Chemical Society, Washington, DC, 1982); J. L. Gole, R. H. Childs, D. A. Dixon, and R. A. Eades, *J. Chem. Phys.* **72**, 6368 (1980).

<sup>19</sup> T. Halicioglu and C. W. Bauschlicher, Jr., *Rep. Prog. Phys.* **51**, 883 (1988).

<sup>20</sup> L. Pauling, *J. Chem. Phys.* **78**, 3346 (1983); C. W. Bauschlicher, Jr., S. P. Walch, and P. E. M. Siegbahn, *J. Chem. Phys.* **78**, 3347 (1983).

<sup>21</sup> S. G. Gagarin and Yu. A. Teterin, *Russ. J. Inorg. Chem.* **29**, 1096 (1984).

<sup>22</sup> C. W. Bauschlicher, Jr., S. R. Langhoff, and P. R. Taylor, *J. Chem. Phys.* **88**, 1041 (1988).

<sup>23</sup> K. Balasubramanian and M. Z. Liao, *Chem. Phys.* **127**, 313 (1988).

<sup>24</sup> C. W. Bauschlicher, Jr., S. R. Langhoff, and H. Partridge, *J. Chem. Phys.* **91**, 2412 (1989); C. W. Bauschlicher, Jr., *Chem. Phys. Lett.* **156**, 91 (1989).

<sup>25</sup> S. P. Walch, C. W. Bauschlicher, Jr., and S. R. Langhoff, *J. Chem. Phys.* **85**, 5900 (1986).

<sup>26</sup> S. R. Langhoff, C. W. Bauschlicher, Jr., S. P. Walch, and B. C. Laskowski, *J. Chem. Phys.* **85**, 7211 (1986).

<sup>27</sup> H. Basch, *J. Am. Chem. Soc.* **103**, 4657 (1981).

<sup>28</sup> K. Balasubramanian, P. Y. Feng, and M. Z. Liao, *J. Chem. Phys.* **91**, 3561 (1989); K. Balasubramanian and P. Y. Feng, *Chem. Phys. Lett.* **159**, 452 (1989).

<sup>29</sup> Y. S. Lee and A. D. McLean, *J. Chem. Phys.* **76**, 735 (1982); R. B. Ross and W. C. Ermler, *ibid.* **89**, 5202 (1985).

<sup>30</sup> J. Demuyne, M.-M. Rohmer, A. Strich, and A. Veillard, *J. Chem. Phys.* **75**, 3443 (1981); R. P. Messmer, T. C. Caves, and C. M. Kao, *J. Chem. Phys. Lett.* **90**, 296 (1982).

<sup>31</sup> S. P. Walch and B. C. Laskowski, *J. Chem. Phys.* **84**, 2743 (1986).

<sup>32</sup> R. C. Baetzold, *J. Chem. Phys.* **68**, 555 (1978).

<sup>33</sup> M. D. Morse, J. B. Hopkins, P. R. R. Langridge-Smith, and R. E. Smalley, *J. Chem. Phys.* **79**, 5316 (1983); E. A. Rohlfing and J. J. Valentini, *ibid.* **84**, 6560 (1986).

<sup>34</sup> R. D. Mead, A. E. Stevens, and W. C. Lineberger, in *Gas Phase Ion Chemistry, Vol. 3. Ions and Light*, edited by M. T. Bowers (Academic, New York, 1984), p. 213.

<sup>35</sup> O. Cheshnovsky, K. J. Taylor, J. Conceicao, and R. E. Smalley, *Phys. Rev. Lett.* **64**, 1785 (1990).

<sup>36</sup> C. S. Feigerle, Ph.D. thesis, University of Colorado, 1983.

<sup>37</sup> D. G. Leopold, K. K. Murray, A. E. Stevens Miller, and W. C. Lineberger, *J. Chem. Phys.* **83**, 4849 (1985).

<sup>38</sup> V. M. Bierbaum, G. B. Ellison, and S. R. Leone, in *Gas Phase Ion Chemistry, Vol. 3. Ions and Light*, edited by M. T. Bowers (Academic, New York, 1984), p. 1.

<sup>39</sup> L. C. Balbas, A. Rubio, J. A. Alonso, and G. Borstel, *Chem. Phys.* **120**,

- 239 (1988).
- <sup>40</sup> G. Hortig and M. Müller, *Z. Phys.* **221**, 119 (1969).
- <sup>41</sup> I. Katasuse, T. Ichihara, Y. Fujita, T. Mastua, T. Sakurai, and H. Matsuta, *Int. J. Mass Spectrom. Ion Process.* **67**, 229 (1985); **74**, 33 (1986).
- <sup>42</sup> H. Hotop and W. C. Lineberger, *J. Phys. Chem. Ref. Data* **14**, 731 (1985).
- <sup>43</sup> C. E. Moore, *Atomic Energy Levels*, Natl. Bur. Stand. (U.S., GPO, Washington, DC, 1952), Circ. 467.
- <sup>44</sup> K. M. Ervin, J. Ho, and W. C. Lineberger, *J. Chem. Phys.* **91**, 5974 (1989).
- <sup>45</sup> G. A. Kerr, N. A. Robertson, J. Hough, and C. N. Man, *Appl. Phys.* **B37**, 11 (1985); R. W. Drever, J. L. Hall, F. V. Kowalski, J. Hough, G. M. Ford, A. J. Munley, and H. Ward, *ibid.* **31**, 97 (1983).
- <sup>46</sup> A. E. Siegman, *Lasers* (University Science Books, Mill Valley, California, 1986); C. Douketis, D. Anex, G. Ewing, and J. P. Reilly, *J. Phys. Chem. Lett.* **13**, 357 (1988); C. E. Tanner, B. P. Masterson, and C. E. Wieman, *Opt. Lett.* **13**, 357 (1988).
- <sup>47</sup> H. Hotop and W. C. Lineberger, *J. Chem. Phys.* **58**, 2379 (1973); H. Hotop, R. A. Bennett, and W. C. Lineberger, *ibid.* **58**, 2373 (1973).
- <sup>48</sup> G. Ganteför, M. Gausa, K.-H. Meiwes-Broer, and H. O. Lutz, *J. Chem. Soc. Faraday Trans.* **86**, 2483 (1990).
- <sup>49</sup> E. Miyoshi, H. Tatewaki, and T. Nakamura, *Int. J. Quantum Chem.* **23**, 1201 (1983); *J. Chem. Phys.* **78**, 815 (1983).
- <sup>50</sup> K. Balasubramanian, *J. Chem. Phys.* **91**, 6585 (1989).
- <sup>51</sup> M. Halmann and I. Laulicht, *J. Chem. Phys.* **43**, 438 (1965); C. Engler, *Z. Phys. Chem. (Leipzig)* **6**, 1193 (1984).
- <sup>52</sup> G. Herzberg, *Molecular Spectra and Molecular Structure I. Spectra of Diatomic Molecules*, 2nd ed. (Van Nostrand Reinhold, New York, 1951).
- <sup>53</sup> P. DiLella, W. Limm, R. H. Lipson, M. Moskovits, and K. V. Taylor, *J. Chem. Phys.* **77**, 5263 (1982).
- <sup>54</sup> M. Broyer, J. Chevalyere, G. Delacretaz, S. Martin, and L. Wöste, *Chem. Phys. Lett.* **99**, 206 (1983); D. G. Leopold and W. C. Lineberger, *J. Chem. Phys.* **85**, 51 (1986); D. G. Leopold, J. Almlöf, W. C. Lineberger, and P. R. Taylor, *ibid.* **88**, 3780 (1988); H. Patridge, D. A. Dixon, S. P. Walch, C. W. Bauschlicher, Jr., and J. L. Gole, *ibid.* **79**, 1859 (1983); H. Patridge, C. W. Bauschlicher, Jr., and P. E. Siegbahn, *Chem. Phys. Lett.* **97**, 198 (1983).
- <sup>55</sup> V. E. Bondybey, *J. Chem. Phys.* **77**, 3771 (1982).
- <sup>56</sup> J. Tellinghuisen, *J. Phys. Chem.* **87**, 5136 (1983); J. Tellinghuisen, in *Photodissociation and Photoionization*, edited by K. P. Lawley (Wiley, New York, 1985).
- <sup>57</sup> Performing the equivalent calculations on the copper and silver dimers with the *ab initio* bond lengths and vibrational frequencies (Ref. 24), we obtain good agreement between calculated and experimental Franck-Condon profiles.
- <sup>58</sup> V. Bonačić-Koutecký, P. Fantucci, and J. Koutecký, *Phys. Rev. B* **37**, 4369 (1988); *J. Chem. Phys.* **91**, 3794 (1989).
- <sup>59</sup> Y. Wang, T. F. George, D. M. Lindsay, and A. C. Beri, *J. Chem. Phys.* **86**, 3593 (1987); D. M. Lindsay, L. Chu, Y. Wang, and T. F. George, *ibid.* **87**, 1685 (1987).
- <sup>60</sup> H. Åkeby, I. Panas, L. G. M. Pettersson, P. Siebahn, and U. Wahlgren, *J. Phys. Chem.* **94**, 5471 (1990).
- <sup>61</sup> M. A. Mitchell and G. A. Ozin, *J. Am. Chem. Soc.* **100**, 6776 (1978).
- <sup>62</sup> D. E. Eastman, *Phys. Rev. B* **2**, 1 (1970); V. S. Fomenko, *Emission Properties of Metals*, 3rd ed. (Naukova Dumka, Kiev., 1970).
- <sup>63</sup> D. M. Wood, *Phys. Rev. Lett.* **46**, 749 (1981).
- <sup>64</sup> N. D. Lang and W. Kohn, *Phys. Rev. B* **1**, 4555 (1970).
- <sup>65</sup> K. M. McHugh, J. G. Eaton, G. H. Lee, H. W. Sarkas, L. H. Kidder, J. T. Snodgrass, M. R. Manaa, and K. H. Bowen, *J. Chem. Phys.* **91**, 3792 (1989).
- <sup>66</sup> K. I. Peterson, P. D. Dao, R. W. Farley, and A. W. Castleman, Jr., *J. Chem. Phys.* **80**, 1780 (1984); T. D. Märk and A. W. Castleman, Jr., *Adv. Atom. Mol. Phys.* **20**, 92 (1985); A. Herrmann, E. Schumacher, and L. Wöste, *J. Chem. Phys.* **68**, 2327 (1978).
- <sup>67</sup> S. W. Wang, *J. Chem. Phys.* **82**, 4633 (1985).
- <sup>68</sup> W. D. Knight, W. A. de Heer, and W. A. Saunders, *Z. Phys. D* **3**, 109 (1986); M. L. Cohen, M. Y. Chou, W. D. Knight, and W. A. de Heer, *J. Phys. Chem.* **91**, 3141 (1987).
- <sup>69</sup> M. M. Kappes, M. Schär, P. Radi, and E. Schumacher, *J. Chem. Phys.* **84**, 1863 (1986).
- <sup>70</sup> W. A. Saunders, Ph.D. thesis, University of California, Berkeley, 1986; K. Clemenger, W. A. de Heer, and W. D. Knight, *Phys. Rev. B* **32**, 1366 (1985).